Journal of Scientific Computing/ manuscript No.
(will be inserted by the editor)

An unconditionally energy stable penalty immersed boundary method for simulating the dynamics of an inextensible interface interacting with a solid particle

Po-Wen Hsieh · Ming-Chih Lai · Suh-Yuh Yang · Cheng-Shu You

Received: August 11, 2013/Revised May 28, 2014/Accepted: –

Abstract In this paper, a novel penalty method based on the immersed boundary formulation is proposed for simulating the transient Stokes flow with an inextensible interface enclosing a suspended solid particle. The main idea of this approach relies on the penalty techniques by modifying the constitutive equation of Stokes flow to weaken the incompressibility condition, relating the surface divergence to the elastic tension σ to relax the interface's inextensibility, and connecting the particle surface-velocity with the particle surface force $\boldsymbol{F}$ to regularize the particle's rigid motion. The advantage of these regularized governing equations is that when they are discretized by the standard centered difference scheme on a staggered grid, the resulting linear system can easily be reduced by eliminating the unknowns p_h, σ_h and $\boldsymbol{F}_h$ directly, so that we just need to solve a smaller linear system of the velocity approximation $\boldsymbol{u}_h$. This advantage is preserved and even enhanced when such approach is applied to the transient Stokes flow with multiple compound vesicles. Moreover, this smaller linear system is symmetric and negative-definite, which enables us to use efficient linear solvers. Another important feature of the proposed method is that the discretization scheme is unconditionally stable in the sense that an appropriately defined energy functional associated with the discrete system is decreasing and hence bounded in time. We numerically test the accuracy and stability of the immersed boundary discretization scheme. The tank-treading and tumbling motions of inextensible interface with a suspended solid particle in the simple shear flow will be studied extensively. The simulation of the motion of multiple compound vesicles will be performed as well. Numerical results illustrate the superior performance of the proposed penalty method.

Keywords immersed boundary method · penalty method · Stokes flow · inextensible interface · solid particle · stability

Po-Wen Hsieh was partially supported by the National Science Council of Taiwan under the grant NSC 102-2115-M-033 -007 -MY2.
Ming-Chih Lai was partially supported by the National Science Council of Taiwan under the grant NSC 101-2115-M-009-014-MY3.
Suh-Yuh Yang was partially supported by the National Science Council of Taiwan under the grant NSC 101-2115-M-008-008-MY2.

Po-Wen Hsieh
Department of Applied Mathematics, Chung Yuan Christian University, Jhongli City, Taoyuan County 32023, Taiwan.
E-mail: pwhsieh0209@gmail.com

Ming-Chih Lai
Center of Mathematical Modeling and Scientific Computing & Department of Applied Mathematics, National Chiao Tung University, Hsinchu 30010, Taiwan.
E-mail: mclai@math.nctu.edu.tw

Suh-Yuh Yang (corresponding author) and Cheng-Shu You
Department of Mathematics, National Central University, Jhongli City, Taoyuan County 32001, Taiwan. Tel.: +886-3-4227151 extension 65130; Fax: +886-3-4257379
E-mail: syyang@math.ncu.edu.tw; csdyou@gmail.com

Mathematics Subject Classification (2000) 65M06 · 65M12 · 76D07 · 76M20

1 Introduction

In recent years, the study of vesicle dynamics has been the focus of intense research. Vesicles provide the simplest model system for simulating complex behavior of biomembranes suspended in the biological fluids. For example, vesicle can be considered as a simplified model for red blood cell in blood flow, since they share many similar characteristic behavior, such as the tank-treading, tumbling and vacillating-breathing (swinging) motions [17] [19]. Basically, such a system consists of two fluids separated by an elastic membrane having the inextensible property, which may be deformed due to the interaction with the biological fluids. Besides, vesicles can also be considered as promising drug carriers for the delivery at specific locations in the organisms [1]. These explain the increasing interest and importance of understanding the vesicle dynamics. In essence, the dynamics of vesicles can be determined by their boundary rigidity, inextensibility, and the hydrodynamical forces.

On the other hand, the immersed boundary (IB) method was introduced by Peskin in the early seventies to model blood flow in the heart and through heart valves. Currently, it has evolved into a simple but powerful method for formulating the coupled equations of motion of a viscous, incompressible fluid with one or more elastic surfaces immersed in the fluid; see [20] and many references therein. In the IB method, an Eulerian description is used for the fluid dynamics, while a Lagrangian form is used for each immersed object. The key idea of the IB method is replacing each suspended object by a suitable contribution to a force density term in the fluid dynamics equations. This allows a single set of fluid dynamics equations to hold in the entire spatial domain without any internal boundary conditions. Moreover, without generating an interface-fitting grid for both exterior and interior regions of each surface at each time step, instead, the IB discretization schemes can be implemented by employing a uniform Cartesian grid over the entire domain and the immersed boundaries are discretized by a set of points that are not constrained to lie on the grid. In the meantime, the Eulerian and Lagrangian variables are linked by interaction equations that involve a smoothed approximation to the Dirac delta function.

Recently, Lai *et al.* [12] developed a fractional step IB method for Stokes flow with an inextensible interface enclosing a suspended solid particle. In addition to solving for the fluid variables, velocity and pressure, the proposed system in [12] involves finding an extra unknown, elastic tension σ, such that the surface divergence of the velocity is vanished along the interface, and an extra unknown, particle surface force $\boldsymbol{F}$, such that the velocity satisfies the no-slip boundary condition along the particle surface. The interface moves with local fluid velocity, while the enclosed particle undergoes a rigid body motion. Finally, the force-free and torque-free conditions along the particle surface are imposed to close the system. They showed that the nullity of the linear algebraic system arising from the centered discretizations of the IB equations over a staggered grid is nonzero, and thus the existence of a solution is guaranteed. They then applied the idea of the fractional step method developed in [23] to solve the resultant linear system of equations. Although the proposed system in [12] seems not to be a satisfactory model for certain biological cells such as the human leukocytes, a lipid bilayer membrane enclosing a fluid with a core, it can be viewed as a heuristic model for developing efficient numerical schemes for analyzing the dynamics of compound vesicles.

In this paper, still based on the formulation of [12], we will propose a novel penalty IB method for the transient Stokes flow problem with an inextensible interface enclosing a suspended solid particle. The main idea of the proposed approach relies on the three penalty techniques. First, we modify the constitutive equation of Stokes flow (cf. [6]) to weaken the incompressibility condition $\nabla \cdot \boldsymbol{u} = 0$ by $\nabla \cdot \boldsymbol{u} + \varepsilon p = 0$ with a small penalty parameter $\varepsilon > 0$. This technique has been well studied in the finite element computation for the incompressible viscous flow problems to circumvent the cumbersome constraint of incompressibility [24]. Second, we assume that the elastic tension σ is given in a specific form to follow the usual Hooke's law for an elastic body [9] [10]. This enables us to relate the surface divergence to the elastic tension such that the interface is relaxed to nearly inextensible. Finally, we connect the particle surface-velocity with the particle surface force $\boldsymbol{F}$ through the use of a virtual particle

to regularize the particle's rigid motion [10]. The advantage of the regularized governing equations is that when they are further discretized by the standard centered difference scheme on a staggered grid, the resulting linear system can easily be reduced by eliminating the unknowns p_h, σ_h and $\boldsymbol{F}_h$ directly so that we just need to solve a smaller linear system of the velocity approximation $\boldsymbol{u}_h$. Moreover, the linear system of $\boldsymbol{u}_h$ is symmetric and negative-definite. This enables us to use efficient solvers, such as the preconditioned conjugate gradient and the algebraic multigrid methods, to find solution of the linear system. We emphasize that this advantage will be preserved and even enhanced when such penalty IB approach is applied to the transient Stokes flow with multiple compound vesicles. Indeed, for multiple vesicle problems, the resulting large linear system of equations is still tractable to block elimination, no matter how many compound vesicles are involved in the fluid, and we only need to solve a reduced system of the velocity. Also, the present approach can be easily extended to Navier-Stokes flow by treating the nonlinear advection terms explicitly in the time integration.

It is well known that the discretizations of the IB equations suffer from a severe time step restriction for maintaining the stability and this time step restriction is typically much more stringent than the one that would be imposed from using explicit differencing techniques; see [2], [4], [14], [20] and [22]. In recent years, considerable effort has been devoted to developing implicit and semi-implicit schemes to alleviate this severe restriction [4] [14] [16] [25]. The instability of these schemes is known not to be a problem related to the advection terms in the incompressible Navier-Stokes equations. Also, it has been pointed out in [18] that discretization schemes need not be fully-implicit in order to achieve unconditional stability. One of important features of the present penalty IB approach is that our semi-implicit discretization scheme for the penalty IB equations is unconditionally stable in the sense that when an appropriately energy functional associated with the discrete system is defined, we can prove that the energy is decreasing, and hence bounded, in time. This result reflects the assertion of [18] in some measure.

Since our penalty IB approach relaxes the interface to be nearly inextensible, it is important to us to measure how extent the inextensibility is conserved as time step advances. In this paper, we will prove that the difference of local stretching factors for two successive time steps is still of first order in time step size Δt, i.e., $O(\Delta t)$. This result is similar to that of [12]. In addition, we find that though the difference of local stretching factors is of first order in time step size, the length of the elastic interface may not be always increasing as much as expected when time step advances. In other words, we could keep the inextensibility of the interface very well. This assertion is very different with [12] and the numerical results reported in Section 5 will support this observation.

We will test the accuracy and stability of the semi-implicit discretization scheme through a number of numerical experiments. The first one, which is quoted from [12], is a Stokes problem without the effects of the inextensible interface and the suspended solid particle. The exact solution of this problem is given and so we can easily compute the errors and estimate the convergence rates. Then we perform a series of numerical simulations for inextensible interface with a suspended solid particle in the simple shear flow. In particular, the tank-treading and tumbling motions will be studied extensively. The simulation of the motion of multiple compound vesicles will be performed as well. Numerical results illustrate the superior performance of the proposed penalty IB approach.

The remainder of this paper is organized as follows. In Section 2, we regularize the governing equations by the penalty techniques. In Section 3, we discretize the IB equations using the standard centered difference scheme on a staggered grid, and the unique solvability of the resulting linear system is also studied. Some advantageous properties of the penalty IB method, including the unconditional stability and the first-order error of inextensibility for two successive time steps, will be derived in Section 4. Numerical results are presented in Section 5. Some concluding remarks are given in Section 6.

2 Regularization of the governing equations of motion

In this paper, we consider a moving immersed inextensible interface Γ enclosing a suspended solid particle P in a two-dimensional fluid domain Ω; see Figure 2.1. We assume that the fluids inside and outside of the interface are the same and governed by the unsteady incompressible Stokes equations, and the interface

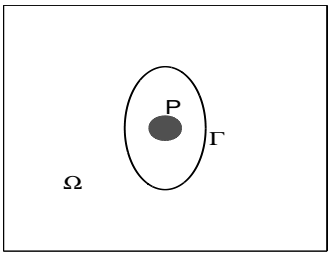

Figure 2.1. A diagram of an inextensible interface Γ enclosing a suspended solid particle P.

is massless and the particle's gravity is neglected. Let the elastic interface Γ and the particle surface ∂P be parameterized by $\boldsymbol{X}(s,t) = (X_1(s,t), X_2(s,t))$ and $\boldsymbol{Y}(\alpha,t) = (Y_1(\alpha,t), Y_2(\alpha,t))$, respectively, where $s \in [0, L_1]$ and $\alpha \in [0, L_2]$ are the corresponding Lagrangian parameters. The governing equations of motion in dimensionless form can be formulated as follows (cf. [12]): for $t > 0$,

$$\frac{\partial \boldsymbol{u}}{\partial t} + \nabla p = \mu \Delta \boldsymbol{u} + \int_\Gamma \frac{\partial(\sigma\boldsymbol{\tau})(s,t)}{\partial s}\delta(\boldsymbol{x} - \boldsymbol{X}(s,t))ds + \int_{\partial P} \boldsymbol{F}(\alpha,t)\delta(\boldsymbol{x} - \boldsymbol{Y}(\alpha,t))d\alpha \quad \text{in } \Omega, \tag{1}$$

$$\nabla \cdot \boldsymbol{u} = 0 \quad \text{in } \Omega, \tag{2}$$

$$\nabla_s \cdot \boldsymbol{U} = \left(\frac{\partial \boldsymbol{U}}{\partial s} \cdot \boldsymbol{\tau}\right)\left|\frac{\partial \boldsymbol{X}}{\partial s}\right|^{-1} = 0 \quad \text{on } \Gamma, \tag{3}$$

$$\frac{\partial \boldsymbol{X}}{\partial t}(s,t) = \boldsymbol{U}(s,t) = \int_\Omega \boldsymbol{u}(\boldsymbol{x},t)\delta(\boldsymbol{x} - \boldsymbol{X}(s,t))d\boldsymbol{x} \quad \text{on } \Gamma, \tag{4}$$

$$\frac{\partial \boldsymbol{Y}}{\partial t}(\alpha,t) = \boldsymbol{V}(\alpha,t) = \int_\Omega \boldsymbol{u}(\boldsymbol{x},t)\delta(\boldsymbol{x} - \boldsymbol{Y}(\alpha,t))d\boldsymbol{x} = \boldsymbol{V}_c + \omega \boldsymbol{r} \quad \text{on } \partial P, \tag{5}$$

$$\int_{\partial P} \boldsymbol{F}(\alpha,t)d\alpha = \boldsymbol{0}, \tag{6}$$

$$\int_{\partial P} \boldsymbol{F}(\alpha,t) \cdot \boldsymbol{r}(\alpha,t)d\alpha = 0, \tag{7}$$

where $\mu > 0$ is the kinematic viscosity, $\boldsymbol{u} = (u, v)$ and p are the velocity field and the pressure, respectively, σ is the elastic tension and $\boldsymbol{F} = (F_1, F_2)$ is the particle surface force, $\boldsymbol{V}_c(t)$ is the translational velocity of the center of particle and $\omega(t)$ is the angular velocity component of the particle, $\boldsymbol{\tau}$ is the unit tangential vector on Γ, $\boldsymbol{r}(\alpha,t) = (-(Y_2(\alpha,t) - Y_{2c}(t)), Y_1(\alpha,t) - Y_{1c}(t))$ is a tangential vector on ∂P, (Y_{1c}, Y_{2c}) is the center of mass of P, $\delta(\boldsymbol{x}) := \delta(x)\delta(y)$ is a two-dimensional Dirac delta function, and $\nabla_s \cdot$ denotes the surface divergence operator.

We note that equations (1) and (2) are the unsteady incompressible Stokes equations with singular force terms arising from the elastic interface and the particle surface. Equations (3) and (4) represent that the interface is inextensible and moves along with the local fluid velocity so that the velocity $\boldsymbol{U}$ is the interpolation of the fluid velocity at the interface. Equation (5) describes the particle surface velocity which is consisted of the translational velocity $\boldsymbol{V}_c$ and the angular velocity ω making the particle moving like a rigid body. Finally, the system of equations will be closed by coupling (6) and (7), which mean the force-free and torque-free conditions for the rigid body motion.

We now introduce the penalty techniques [6] [9] [10] [24] to regularize equations (2), (3) and (5). First, by modifying the constitutive equation of Stokes flow (cf. [6]), we are able to weaken the incompressibility condition $\nabla \cdot \boldsymbol{u} = 0$ in Ω by

$$\nabla \cdot \boldsymbol{u} + \varepsilon p = 0 \quad \text{in } \Omega, \tag{8}$$

where $\varepsilon > 0$ is a small penalty parameter. This penalty technique has been well studied in the finite element computation for the incompressible Stokes equations. For example, it has been shown that the

solution $(\boldsymbol{u}_\varepsilon, p_\varepsilon)$ of the penalty approach will converge to the Stokes solution $(\boldsymbol{u}, p)$ in some suitable norms as $\varepsilon \to 0^+$. More precisely, we have

$$\boldsymbol{u}_\varepsilon \to \boldsymbol{u} \text{ in the } H^1(\Omega) \text{ norm and } p_\varepsilon \to p \text{ in the } L^2(\Omega) \text{ norm as } \varepsilon \to 0^+.$$

For the theoretical analysis, we refer the reader to [24] for more details. In the practical computation, an appropriate choice of the parameter ε has been suggested by Hughes *et al.* [6] that $\varepsilon = 1/(c\widetilde{\mu})$, where $\widetilde{\mu}$ is the dynamic viscosity and the constant c is taken as $c = 10^7$ for Stokes flow. They pointed out that the choice of c seems to be problem independent. This is consistent with our numerical experience.

Second, based on the Hooke's law, we assume that the elastic tension σ is given in the form

$$\sigma(s,t) = \sigma_0\Big(\Big|\frac{\partial \boldsymbol{X}}{\partial s}(s,t)\Big| - \Big|\frac{\partial \boldsymbol{X}}{\partial s}(s,0)\Big|\Big), \tag{9}$$

with a sufficiently large elastic coefficient σ_0. Since σ_0 is large, the length of the tangential vector $\partial \boldsymbol{X}(s,t)/\partial s$ will be always close to the initial length, i.e.,

$$\Big|\frac{\partial \boldsymbol{X}}{\partial s}(s,t)\Big| \approx \Big|\frac{\partial \boldsymbol{X}}{\partial s}(s,0)\Big| \quad \text{for all } s \in [0, L_1] \text{ and } t > 0.$$

In other words, the interface is no longer exactly inextensible. Instead, the elastic interface is allowed to be nearly inextensible. Indeed, from [13], we have

$$\frac{\partial}{\partial t}\Big|\frac{\partial \boldsymbol{X}}{\partial s}\Big| = (\nabla_s \cdot \boldsymbol{U})\Big|\frac{\partial \boldsymbol{X}}{\partial s}\Big|. \tag{10}$$

Combining (9) with (10), the surface divergence free equation (3) should be replaced by

$$\Big(\frac{\partial \boldsymbol{U}}{\partial s} \cdot \boldsymbol{\tau}\Big)\Big|\frac{\partial \boldsymbol{X}}{\partial s}\Big|^{-1} = \nabla_s \cdot \boldsymbol{U} = \frac{1}{\sigma_0}\frac{\partial \sigma}{\partial t}\Big|\frac{\partial \boldsymbol{X}}{\partial s}\Big|^{-1} \quad \text{on } \Gamma. \tag{11}$$

In other words, we obtain

$$\frac{\partial \sigma}{\partial t} = \sigma_0\left(\frac{\partial \boldsymbol{U}}{\partial s} \cdot \boldsymbol{\tau}\right) \quad \text{on } \Gamma. \tag{12}$$

To sum up, assumption (9) relates the surface divergence with the elastic tension σ, as that given in (11), such that the interface is allowed to be nearly inextensible.

Finally, following the Hooke's law again, we assume that

$$\boldsymbol{F} = k_0(\boldsymbol{Y} - \widetilde{\boldsymbol{Y}}), \tag{13}$$

with a sufficiently large stiffness constant k_0, where $\widetilde{\boldsymbol{Y}}$ is the parametrization of the virtual solid particle $\widetilde{P}$ and $\widetilde{\boldsymbol{Y}}$ is assumed to have the same parametric variable α with $\boldsymbol{Y}$ in the same interval $[0, L_2]$. The significance of this assumption can be interpreted as follows. When the flow hits the solid particle, we image that the particle surface may be deformed a little bit to $\widetilde{\boldsymbol{Y}}$ but at the same moment, the reacting force $\boldsymbol{F}$ pulls it back to $\boldsymbol{Y}$, a real position of the particle surface; see Figure 2.2. Since k_0 is large, $\boldsymbol{Y}(\alpha,t) \approx \widetilde{\boldsymbol{Y}}(\alpha,t)$ for all $\alpha \in [0, L_2]$ and $t > 0$. Under assumption (13) with the equation of rigid motion of $\widetilde{\boldsymbol{Y}}$,

$$\frac{\partial \widetilde{\boldsymbol{Y}}}{\partial t} = \widetilde{\boldsymbol{V}} = \boldsymbol{V}_c + \omega \widetilde{\boldsymbol{r}}, \tag{14}$$

we have, combining with (5),

$$\frac{\partial \boldsymbol{F}}{\partial t} = k_0\left(\frac{\partial \boldsymbol{Y}}{\partial t} - \frac{\partial \widetilde{\boldsymbol{Y}}}{\partial t}\right) = k_0(\boldsymbol{V} - \widetilde{\boldsymbol{V}}) = k_0(\boldsymbol{V}_c + \omega \boldsymbol{r} - \widetilde{\boldsymbol{V}}) \quad \text{on } \partial\widetilde{P}. \tag{15}$$

Consequently, we connect the particle surface-velocity $\boldsymbol{V}$ with the particle surface force $\boldsymbol{F}$ by (15). This enables us to regularize the particle's rigid motion, see (19) and (23) below.

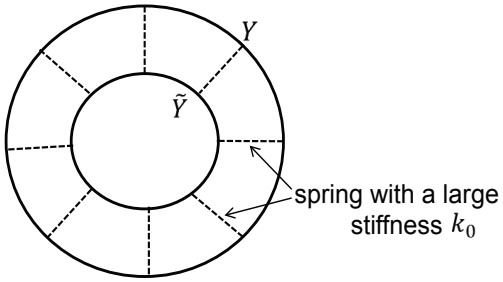

Figure 2.2. The reacting force $\boldsymbol{F}$ pulls $\widetilde{\boldsymbol{Y}}$ back to target position $\boldsymbol{Y}$.

In summary, we obtain the following system of equations, which models the dynamics of a nearly inextensible vesicle enclosing a suspended solid particle in Stokes flow: for $t > 0$,

$$\frac{\partial \boldsymbol{u}}{\partial t} + \nabla p = \mu \Delta \boldsymbol{u} + \int_{\Gamma} \frac{\partial (\sigma \boldsymbol{\tau})(s,t)}{\partial s} \delta(\boldsymbol{x} - \boldsymbol{X}(s,t)) ds + \int_{\partial P} \boldsymbol{F}(\alpha,t) \delta(\boldsymbol{x} - \boldsymbol{Y}(\alpha,t)) d\alpha \quad \text{in } \Omega, \tag{16}$$

$$\nabla \cdot \boldsymbol{u} + \varepsilon p = 0 \quad \text{in } \Omega, \tag{17}$$

$$\frac{\partial \sigma}{\partial t} = \sigma_0 \left(\frac{\partial \boldsymbol{U}}{\partial s} \cdot \boldsymbol{\tau} \right) \quad \text{on } \Gamma, \tag{18}$$

$$\frac{\partial \boldsymbol{F}}{\partial t} = k_0 (\boldsymbol{V}_c + \omega \boldsymbol{r} - \widetilde{\boldsymbol{V}}) \quad \text{on } \partial \widetilde{P}, \tag{19}$$

$$\int_{\partial P} \boldsymbol{F}(\alpha,t) d\alpha = \boldsymbol{0}, \tag{20}$$

$$\int_{\partial P} \boldsymbol{F}(\alpha,t) \cdot \boldsymbol{r}(\alpha,t) d\alpha = 0, \tag{21}$$

$$\frac{\partial \boldsymbol{X}}{\partial t}(s,t) = \boldsymbol{U}(s,t) = \int_{\Omega} \boldsymbol{u}(\boldsymbol{x},t) \delta(\boldsymbol{x} - \boldsymbol{X}(s,t)) d\boldsymbol{x} \quad \text{on } \Gamma, \tag{22}$$

$$\widetilde{\boldsymbol{V}}(\alpha,t) = \int_{\Omega} \boldsymbol{u}(\boldsymbol{x},t) \delta(\boldsymbol{x} - (\boldsymbol{Y}(\alpha,t) - \frac{1}{k_0} \boldsymbol{F}(\alpha,t))) d\boldsymbol{x} \quad \text{on } \partial \widetilde{P}, \tag{23}$$

where ε is small but σ_0 and k_0 are large enough, and $\partial \widetilde{P}$ denotes the surface of the virtual solid particle $\widetilde{P}$, which is parameterized by $\widetilde{\boldsymbol{Y}}(\alpha,t) = (\widetilde{Y}_1(\alpha,t), \widetilde{Y}_2(\alpha,t)) = \boldsymbol{Y}(\alpha,t) - (1/k_0)\boldsymbol{F}(\alpha,t)$ for $\alpha \in [0, L_2]$.

3 Discretizations of the immersed boundary equations

In this section, we are going to apply the second-order centered difference scheme to discretize the immersed boundary equations (16)-(23) to reach a linear algebraic system. For simplicity, we assume that the computational domain is a rectangular region $\Omega = [a,b] \times [c,d]$ and that the fluid variables are defined on the staggered marker-and-cell (MAC) grids [5]. As shown in Figure 3.1, we define the pressure on the grid points $(x_i, y_j) = (a + (i-1/2)\Delta x, c + (j-1/2)\Delta y)$ for $1 \le i \le m_x$ and $1 \le j \le m_y$, while the velocity components u and v are defined at $(x_{i-1/2}, y_j) = (a + (i-1)\Delta x, c + (j-1/2)\Delta y)$ for $1 \le i \le m_x + 1$ and $1 \le j \le m_y$ and $(x_i, y_{j-1/2}) = (a + (i-1/2)\Delta x, c + (j-1)\Delta y)$ for $1 \le i \le m_x$ and $1 \le j \le m_y + 1$, respectively. Here, we use a uniform mesh with mesh size $h = \Delta x = \Delta y$.

For the immersed nearly inextensible elastic interface $\boldsymbol{X}$ at a given time, we use the Lagrangian markers $\boldsymbol{X}_k = \boldsymbol{X}(s_k)$, where $s_k = k\Delta s$ for $k = 0, 1, \cdots, M_e$, and Δs is roughly chosen as a half of fluid mesh size h. Since the elastic interface is closed, we have $\boldsymbol{X}_0 = \boldsymbol{X}_{M_e}$. We remark that these points will be used in the computation of the values of the discrete delta functions. The elastic tension is defined on the "half-integer" points given by $s_{k-1/2} = (k-1/2)\Delta s$, so we denote it by $\sigma_{k-1/2}$. Similarly, we use the

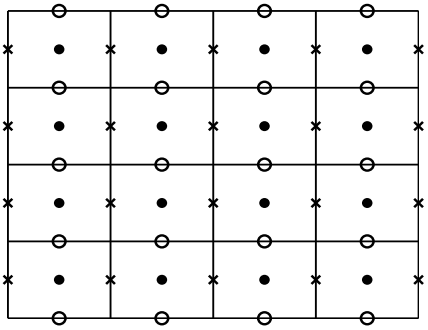

Figure 3.1. A schematic diagram of the computational domain Ω with staggered grid, where the unknowns u, v and p are approximated at the grid points marked by $\times$, $\circ$ and $\bullet$, respectively.

Lagrangian markers $\boldsymbol{Y}_k = \boldsymbol{Y}(\alpha_k)$ on particle surface with $\alpha_k = k\Delta\alpha$, $k = 0, 1, \cdots, M_p$, and $\Delta\alpha$ is also roughly chosen as a half of fluid mesh size h.

In what follows, the discrete spatial operators ∇_h, Δ_h, and $\nabla_{sh}\cdot$ denote the standard second-order centered difference approximations to the gradient, Laplacian and surface divergence operators, respectively. For any function $\psi(s)$ defined on the interface Γ, we approximate the partial derivative $\partial\psi/\partial s$ by the centered difference scheme as

$$D_s\psi(s) = \frac{\psi(s + \Delta s/2) - \psi(s - \Delta s/2)}{\Delta s}.$$

Thus, the interface stretching factor $|\partial\boldsymbol{X}/\partial s|$ and the unit tangent $\boldsymbol{\tau}$ can be approximated by $|D_s\boldsymbol{X}|$ and $D_s\boldsymbol{X}/|D_s\boldsymbol{X}|$, which are defined at the half-integer points. We denote them by $|D_s\boldsymbol{X}|_{k-1/2}$ and $\boldsymbol{\tau}_{k-1/2}$, respectively.

Let Δt be the time step size, and the superscript of the variables denote the time step index. At the beginning of each time step n, the elastic tension $\sigma^n_{k-1/2}$, the particle surface force $\boldsymbol{F}^n_k$, the interface configuration $\boldsymbol{X}^n_k$, the particle surface $\boldsymbol{Y}^n_k = (Y^n_{1k}, Y^n_{2k})$, and its center $\boldsymbol{Y}^n_c = (Y^n_{1c}, Y^n_{2c})$ are all given. Despite the face that the problem is non-linear, here we propose a linearly semi-implicit difference scheme for the system of equations (16)-(23). The time step can be advanced as follows:

$$-\frac{\boldsymbol{u}^{n+1} - \boldsymbol{u}^n}{\Delta t} + \mu\Delta_h\boldsymbol{u}^{n+1} - \nabla_h p^{n+1} + \sum_{k=1}^{M_e} D_s(\sigma^{n+1}\boldsymbol{\tau}^n)_k\delta_h(\boldsymbol{x} - \boldsymbol{X}^n_k)\Delta s + \sum_{k=1}^{M_p} \boldsymbol{F}^{n+1}_k\delta_h(\boldsymbol{x} - \boldsymbol{Y}^n_k)\Delta\alpha = \boldsymbol{0}, \tag{24}$$

$$\nabla_h \cdot \boldsymbol{u}^{n+1} + \varepsilon p^{n+1} = 0, \tag{25}$$

$$\frac{\sigma^{n+1}_{k-1/2} - \sigma^n_{k-1/2}}{\Delta t} - \sigma_0\frac{\boldsymbol{U}^{n+1}_k - \boldsymbol{U}^{n+1}_{k-1}}{\Delta s}\cdot\boldsymbol{\tau}^n_{k-1/2} = 0, \tag{26}$$

$$\frac{\boldsymbol{F}^{n+1}_k - \boldsymbol{F}^n_k}{\Delta t} - k_0\left(\boldsymbol{V}^{n+1}_c + \omega^{n+1}\begin{bmatrix} -(Y^n_{2k} - Y^n_{2c}) \\ Y^n_{1k} - Y^n_{1c}\end{bmatrix} - \widetilde{\boldsymbol{V}}^{n+1}_k\right) = \boldsymbol{0}, \tag{27}$$

$$\sum_{k=1}^{M_p} \boldsymbol{F}^{n+1}_k\Delta\alpha = \boldsymbol{0}, \tag{28}$$

$$\sum_{k=1}^{M_p}\Big(F^{n+1}_{1k}(Y^n_{2k} - Y^n_{2c}) - F^{n+1}_{2k}(Y^n_{1k} - Y^l_{1c})\Big)\Delta\alpha = 0, \tag{29}$$

$$\frac{\boldsymbol{X}_k^{n+1}-\boldsymbol{X}_k^n}{\Delta t}=\boldsymbol{U}_k^{n+1}=\sum_{\boldsymbol{x}}\boldsymbol{u}^{n+1}(\boldsymbol{x})\delta_h(\boldsymbol{x}-\boldsymbol{X}_k^n)h^2, \tag{30}$$

$$\widetilde{\boldsymbol{V}}_k^{n+1}=\sum_{\boldsymbol{x}}\boldsymbol{u}^{n+1}(\boldsymbol{x})\delta_h(\boldsymbol{x}-\boldsymbol{Y}_k^n+\frac{1}{k_0}\boldsymbol{F}_k^n)h^2. \tag{31}$$

We remark that since the stiffness constant k_0 is large, in practical computation, we may use $\delta_h(\boldsymbol{x}-\boldsymbol{Y}_k^n)$ to replace the term $\delta_h(\boldsymbol{x}-\boldsymbol{Y}_k^n+\frac{1}{k_0}\boldsymbol{F}_k^n)$ in (31). For the computation of the discrete delta function $\delta_h(\boldsymbol{x})$, we adopt the following smoother version developed in [28],

$$\delta_h(x,y)=\frac{1}{h^2}\phi\Big(\frac{x}{h}\Big)\phi\Big(\frac{y}{h}\Big), \tag{32}$$

$$\phi(\xi)=\begin{cases}\frac{3}{8}+\frac{\pi}{32}-\frac{\xi^2}{4}, & |\xi|<0.5,\\ \frac{1}{4}+\frac{1-|\xi|}{8}\sqrt{-2+8|\xi|-4\xi^2}-\frac{1}{8}\sin^{-1}(\sqrt{2}(|\xi|-1)), & 0.5\le|\xi|\le 1.5,\\ \frac{17}{16}-\frac{\pi}{64}-\frac{3|\xi|}{4}+\frac{\xi^2}{8}+\frac{|\xi|-2}{16}\sqrt{-14+16|\xi|-4\xi^2} & \\ \quad+\frac{1}{16}\sin^{-1}(\sqrt{2}(|\xi|-2)), & 1.5\le|\xi|\le 2.5,\\ 0, & 2.5\le|\xi|.\end{cases} \tag{33}$$

Now, using the staggered grid for the fluid variables, the matrix obtained by the discrete divergence of the fluid velocity can be written as the transpose of the discrete gradient of the pressure. The matrix produced by the discrete surface divergence of the velocity can be written as the transpose of the matrix obtained by the discrete spreading operator of the tension with some suitable rescaling. Similarly, the matrix obtained by the discrete spreading operator of the force arising from the suspended solid particle boundary can be written as the transpose of the matrix obtained by the discrete interpolating operator of velocity with some suitable rescaling; see [12] and also the discrete skew-adjoint and adjoint properties given in Section 4 below. Thus, the resulting linear system assembled from (24)-(31) is symmetric and can be written as

$$\begin{bmatrix}A & B & S & E & 0\\ B^\top & \varepsilon I & 0 & 0 & 0\\ S^\top & 0 & \varepsilon_1 I & 0 & 0\\ E^\top & 0 & 0 & \varepsilon_2 I & R\\ 0 & 0 & 0 & R^\top & 0\end{bmatrix}\begin{bmatrix}\boldsymbol{u}_h^{n+1}\\ p_h^{n+1}\\ \sigma_h^{n+1}\\ \boldsymbol{F}_h^{n+1}\\ \boldsymbol{\Theta}_h^{n+1}\end{bmatrix}=\begin{bmatrix}\boldsymbol{c}_1\\ c_2\\ m_\sigma\\ \boldsymbol{m}_{\boldsymbol{F}}\\ \boldsymbol{0}\end{bmatrix}, \tag{34}$$

where $\varepsilon_1=\Delta s/(\sigma_0 h^2\Delta t)$, $\varepsilon_2=\Delta\alpha/(k_0 h^2\Delta t)$, ψ_h^{n+1} denotes the unknown vector value of ψ at the corresponding grid points, and $\boldsymbol{\Theta}:=(V_{1c},V_{2c},\omega)$. The submatrices A, B, S, E, and R respectively represent the discrete Laplacian-like operator, $\mu\Delta_h-(1/\Delta t)I$, the discrete gradient operator, $-\nabla_h$, the discrete spreading operator on tension, the discrete spreading operator on the surface force, and the discrete rigid body motion equation. In the right-hand side of (34), $\boldsymbol{c}_1$ comes from the boundary condition and $\boldsymbol{u}_h^n$, c_2 consists only of the velocity boundary conditions since the pressure is evaluated at each cell center, m_σ and $\boldsymbol{m}_{\boldsymbol{F}}$ are depending on σ_h^n and $\boldsymbol{F}_h^n$, respectively.

In general, (34) is a large linear system and it is cost-ineffective to solve it directly even if it is a sparse one. We propose an alternative way to efficiently solve the system as follows. From (34), we obviously have $p_h^{n+1}=(1/\varepsilon)(c_2-B^\top\boldsymbol{u}_h^{n+1})$ and $\sigma_h^{n+1}=(1/\varepsilon_1)(m_\sigma-S^\top\boldsymbol{u}_h^{n+1})$. In addition, $R^\top\boldsymbol{F}_h^{n+1}=\boldsymbol{0}$ and $E^\top\boldsymbol{u}_h^{n+1}+\varepsilon_2\boldsymbol{F}_h^{n+1}+R\boldsymbol{\Theta}_h^{n+1}=\boldsymbol{m}_{\boldsymbol{F}}$ easily imply

$$R^\top E^\top\boldsymbol{u}_h^{n+1}+R^\top R\boldsymbol{\Theta}_h^{n+1}=R^\top\boldsymbol{m}_{\boldsymbol{F}}. \tag{35}$$

We will show the invertibility of the 3×3 matrix $R^\top R$ later and after that we obtain

$$\boldsymbol{\Theta}_h^{n+1}=(R^\top R)^{-1}R^\top(\boldsymbol{m}_{\boldsymbol{F}}-E^\top\boldsymbol{u}_h^{n+1}), \tag{36}$$

and then

$$\boldsymbol{F}_h^{n+1}=\frac{1}{\varepsilon_2}\Big((I-R(R^\top R)^{-1}R^\top)\boldsymbol{m}_{\boldsymbol{F}}-(I-R(R^\top R)^{-1}R^\top)E^\top\boldsymbol{u}_h^{n+1}\Big). \tag{37}$$

Therefore, the linear system (34) can be reduced into a smaller one:

$$\widetilde{A}\boldsymbol{u}_h^{n+1} = \boldsymbol{b}, \tag{38}$$

where the matrix $\widetilde{A}$ and the right-hand side vector $\boldsymbol{b}$ are defined as

$$\widetilde{A} := A - \frac{1}{\varepsilon}BB^\top - \frac{1}{\varepsilon_1}SS^\top - \frac{1}{\varepsilon_2}E(I - R(R^\top R)^{-1}R^\top)E^\top, \tag{39}$$

$$\boldsymbol{b} := \boldsymbol{c}_1 - \frac{1}{\varepsilon}Bc_2 - \frac{1}{\varepsilon_1}Sm_\sigma - \frac{1}{\varepsilon_2}E(I - R(R^\top R)^{-1}R^\top)\boldsymbol{m_F}. \tag{40}$$

We now show the invertibility of the 3×3 matrix $R^\top R$. First, the matrix R assembled from (27) can be written as

$$R = -\frac{\Delta\alpha}{h^2}\begin{bmatrix} 1 & 0 & -(Y_{21}^n - Y_{2c}^n) \\ \vdots & \vdots & \vdots \\ 1 & 0 & -(Y_{2M_p}^n - Y_{2c}^n) \\ 0 & 1 & (Y_{11}^n - Y_{1c}^n) \\ \vdots & \vdots & \vdots \\ 0 & 1 & (Y_{1M_p}^n - Y_{1c}^n) \end{bmatrix}.$$

To simplify the notation, we define $a_k = Y_{1k}^n - Y_{1c}^n$ and $b_k = Y_{2k}^n - Y_{2c}^n$. Then we have

$$\begin{aligned}
\left(\frac{h^4}{\Delta\alpha^2}\right)^3 \det(R^\top R) &= \det\begin{bmatrix} M_p & 0 & -\sum_{k=1}^{M_p} b_k \\ 0 & M_p & \sum_{k=1}^{M_p} a_k \\ -\sum_{k=1}^{M_p} b_k & \sum_{k=1}^{M_p} a_k & \sum_{k=1}^{M_p} a_k^2 + \sum_{k=1}^{M_p} b_k^2 \end{bmatrix} \\
&= M_p\left\{M_p\sum_{k=1}^{M_p} a_k^2 + M_p\sum_{k=1}^{M_p} b_k^2 - \left(\sum_{k=1}^{M_p} a_k\right)^2 - \left(\sum_{k=1}^{M_p} b_k\right)^2\right\} \\
&\text{(by Cauchy-Schwarz inequality)} \\
&\geq M_p\left\{M_p\sum_{k=1}^{M_p} a_k^2 + M_p\sum_{k=1}^{M_p} b_k^2 - \left(\sum_{k=1}^{M_p} a_k^2\right)\left(\sum_{k=1}^{M_p} 1^2\right) - \left(\sum_{k=1}^{M_p} b_k^2\right)\left(\sum_{k=1}^{M_p} 1^2\right)\right\} \\
&= M_p\left\{M_p\sum_{k=1}^{M_p} a_k^2 + M_p\sum_{k=1}^{M_p} b_k^2 - M_p\sum_{k=1}^{M_p} a_k^2 - M_p\sum_{k=1}^{M_p} b_k^2\right\} = 0,
\end{aligned}$$

where the equality holds in Cauchy-Schwarz inequality if and only if $a_k = C_1$ and $b_k = C_2$ for all $k = 1, 2, \cdots, M_p$ and for some constants C_1 and C_2, both independent of k. However, it it will never occur in our case. This leads to $\det(R^\top R) > 0$, and thus $R^\top R$ is invertible. Note that we can efficiently compute the inverse of $R^\top R$ because it is only a 3×3 matrix. Furthermore, we can show the following result:

Theorem 3.1. *The matrix $\widetilde{A}$ is symmetric and negative-definite.*

Proof. It is obvious that matrix $\widetilde{A}$ is symmetric. Using the facts that A is negative-definite and both $BB^\top$ and $SS^\top$ are positive semi-definite, we only need to show that $I - R(R^\top R)^{-1}R^\top$ is a positive semi-definite matrix. A direct computation,

$$(I - R(R^\top R)^{-1}R^\top)(I - R(R^\top R)^{-1}R^\top) = I - R(R^\top R)^{-1}R^\top, \tag{41}$$

shows that $I - R(R^\top R)^{-1}R^\top$ is a projection matrix, and then its eigenvalues should be 0 or 1. This leads to the assertion and thus completes the proof. □

Thanks to this property of matrix $\widetilde{A}$, we can solve (38) by using some efficient linear solvers, such as the preconditioned conjugate gradient and the algebraic multigrid methods.

Once we obtain the new velocity field $\boldsymbol{u}^{n+1}$ on the fluid grid, we can interpolate the new velocity to the marker points by (30) and move the Lagrangian markers to new positions by

$$\boldsymbol{X}_k^{n+1} = \boldsymbol{X}_k^n + \Delta t \boldsymbol{U}_k^{n+1}. \tag{42}$$

For the solid particle motion, the particle center velocity $\boldsymbol{V}_c$ and the angular velocity component ω will be obtained by (36). Instead of first using the interpolation formula to find the new velocity and then updating the particle surface points, we simply adopt the idea of rigid body motion to determine the particle surface position (cf. [12]). Indeed, we compute the new particle center and the rotational angle by

$$\boldsymbol{Y}_c^{n+1} = \boldsymbol{Y}_c^n + \Delta t \boldsymbol{V}_c^{n+1}, \qquad \theta^{n+1} = \theta^n + \Delta t \omega^{n+1} \tag{43}$$

and use them to determine the new particle surface position as

$$\boldsymbol{Y}_k^{n+1} = \boldsymbol{Y}_c^{n+1} + \begin{bmatrix} \cos\theta^{n+1} & -\sin\theta^{n+1} \\ \sin\theta^{n+1} & \cos\theta^{n+1} \end{bmatrix} \boldsymbol{Y}_k^0. \tag{44}$$

Finally, we remark that the proposed penalty IB approach can be applied to the transient Stokes flow with multiple compound vesicles as well. Similar to the above procedure, the resulting large linear system of equations is still tractable to block elimination, no matter how many compound vesicles are involved in the fluid, so that we only need to solve a reduced system with the velocity being the single unknown. Consequently, for multiple vesicle problems, the computational cost of the proposed penalty method is mainly devoted to solving a reduced linear system of the velocity approximation at each time step. This is one of the advantageous features of the proposed method.

4 Properties of the penalty immersed boundary method

In this section, we will discuss some properties of the penalty IB method.

4.1. Skew-adjointness and adjointness in the continuous case

Let us first define the following spreading operators $S_1(\sigma)$ and $S_2(\boldsymbol{F})$ and the inner products of functions on Ω, Γ and ∂P:

$$S_1(\sigma) = \int_\Gamma \frac{\partial}{\partial s}(\sigma\boldsymbol{\tau})\delta(\mathbf{x} - \boldsymbol{X}(s,t))ds, \qquad S_2(\boldsymbol{F}) = \int_{\partial P} \boldsymbol{F}\delta(\boldsymbol{x} - \boldsymbol{Y}(\alpha,t))d\alpha,$$

$$\mathcal{T}_1(\boldsymbol{u}) = \frac{\partial \boldsymbol{U}}{\partial s}\cdot\boldsymbol{\tau}, \qquad \mathcal{T}_2(\boldsymbol{u}) = \int_\Omega \boldsymbol{u}(\boldsymbol{x})\delta(\boldsymbol{x} - \boldsymbol{Y}(\alpha,t))d\boldsymbol{x},$$

$$\langle \boldsymbol{u}, \boldsymbol{v}\rangle_\Omega = \int_\Omega \boldsymbol{u}\cdot\boldsymbol{v}d\boldsymbol{x}, \qquad \langle f, g\rangle_\Gamma = \int_\Gamma f(s)g(s)ds, \qquad \langle \phi, \varphi\rangle_{\partial P} = \int_{\partial P}\phi(\alpha)\varphi(\alpha)d\alpha.$$

Then we have

$$\begin{aligned}
\langle S_1(\sigma), \boldsymbol{u}\rangle_\Omega &= \int_\Omega \left(\int_\Gamma \frac{\partial}{\partial s}(\sigma\boldsymbol{\tau})\delta(\boldsymbol{x} - \boldsymbol{X}(s,t))ds \right)\cdot \boldsymbol{u}(\boldsymbol{x})d\boldsymbol{x} \\
&= \int_\Gamma \frac{\partial}{\partial s}(\sigma\boldsymbol{\tau})\cdot\left(\int_\Omega \boldsymbol{u}(\boldsymbol{x})\delta(\boldsymbol{x} - \boldsymbol{X}(s,t))d\boldsymbol{x} \right) ds \\
&= -\int_\Gamma \sigma\left(\boldsymbol{\tau}\cdot\frac{\partial \boldsymbol{U}}{\partial s} \right) ds = \langle \sigma, -\mathcal{T}_1(\boldsymbol{u})\rangle_\Gamma,
\end{aligned} \tag{45}$$

which means that S_1 and $\mathcal{T}_1$ are skew-adjoint. We also have

$$\begin{aligned}\langle S_2(\boldsymbol{F}), \boldsymbol{u}\rangle_\Omega &= \int_\Omega \left(\int_{\partial P} \boldsymbol{F}\delta(\boldsymbol{x}-\boldsymbol{Y}(\alpha,t))d\alpha\right)\cdot \boldsymbol{u}(\boldsymbol{x})d\boldsymbol{x}\\ &= \int_{\partial P} \boldsymbol{F}\cdot\left(\int_\Omega \boldsymbol{u}(\boldsymbol{x})\delta(\boldsymbol{x}-\boldsymbol{Y}(\alpha,t))d\boldsymbol{x}\right)d\alpha\\ &= \langle \boldsymbol{F}, \boldsymbol{V}\rangle_{\partial P} = \langle \boldsymbol{F}, \mathcal{T}_2(\boldsymbol{u})\rangle_{\partial P},\end{aligned} \tag{46}$$

that is, S_2 and $\mathcal{T}_2$ are adjoint. Moreover, since we assume the elastic tension and the particle surface force in the form

$$\begin{aligned}\sigma(s,t) &= \sigma_0\Big(\Big|\frac{\partial \boldsymbol{X}}{\partial s}(s,t)\Big| - \Big|\frac{\partial \boldsymbol{X}}{\partial s}(s,0)\Big|\Big),\\ \boldsymbol{F} &= k_0(\boldsymbol{Y}-\widetilde{\boldsymbol{Y}}),\end{aligned}$$

the associated potential energies are given by

$$\mathcal{E}_\sigma(t) = \int_\Gamma \frac{\sigma_0}{2}\Big(\Big|\frac{\partial \boldsymbol{X}}{\partial s}(s,t)\Big| - \Big|\frac{\partial \boldsymbol{X}}{\partial s}(s,0)\Big|\Big)^2 ds, \tag{47}$$

$$\mathcal{E}_{\boldsymbol{F}}(t) = \int_{\partial P} \frac{k_0}{2}|\boldsymbol{Y}(\alpha,t)-\widetilde{\boldsymbol{Y}}(\alpha,t)|^2 d\alpha. \tag{48}$$

Therefore, combining (47) with (45) and (18), and (46) with (20) and (21), we have

$$\begin{aligned}\frac{d\mathcal{E}_\sigma}{dt} &= \int_\Gamma \frac{1}{2\sigma_0}\frac{\partial \sigma^2}{\partial t}ds = \int_\Gamma \sigma\Big(\frac{1}{\sigma_0}\frac{\partial \sigma}{\partial t}\Big)ds\\ &= \int_\Gamma \sigma\Big(\boldsymbol{\tau}\cdot\frac{\partial \boldsymbol{U}}{\partial s}\Big)ds = -\langle S_1(\sigma), \boldsymbol{u}\rangle_\Omega\end{aligned} \tag{49}$$

and

$$\langle S_2(\boldsymbol{F}), \boldsymbol{u}\rangle_\Omega = \langle \boldsymbol{F}, \boldsymbol{V}\rangle_{\partial P} = \langle \boldsymbol{F}, \boldsymbol{V}_c + \omega \boldsymbol{r}\rangle_{\partial P} = \boldsymbol{V}_c\cdot\langle \boldsymbol{F}, \boldsymbol{1}\rangle_{\partial P} + \omega\langle \boldsymbol{F}, \boldsymbol{r}\rangle_{\partial P} = 0. \tag{50}$$

From (50) and (19), we obtain

$$\langle \boldsymbol{F}, \widetilde{\boldsymbol{V}} + \frac{1}{k_0}\frac{\partial \boldsymbol{F}}{\partial t}\rangle_{\partial P} = 0,$$

which leads to

$$\frac{d\mathcal{E}_{\boldsymbol{F}}}{dt} = \langle \boldsymbol{F}, \frac{1}{k_0}\frac{\partial \boldsymbol{F}}{\partial t}\rangle_{\partial P} = -\langle \boldsymbol{F}, \widetilde{\boldsymbol{V}}\rangle_{\partial P}. \tag{51}$$

According to (49) and (51), we can conclude that the negative rate of change of potential energy of the elastic interface is equal to the work done by the interface on the fluid, while the work done by surface force $\boldsymbol{F}$ pulling the virtual solid particle, characterized by $\widetilde{\boldsymbol{Y}}$, back to the true particle position $\boldsymbol{Y}$ equals the negative rate of change of potential energy of the particle.

4.2. Skew-adjointness and adjointness in the discrete case

We first define the following discrete operators S_{1h}, S_{2h}, $\mathcal{T}_{1h}$, $\mathcal{T}_{2h}$, and discrete inner products:

$$S_{1h}(\sigma^{n+1}) = \sum_k D_s(\sigma^{n+1}\boldsymbol{\tau}^n)_k\delta_h(\boldsymbol{x}-\boldsymbol{X}_k^n)\Delta s, \qquad S_{2h}(\boldsymbol{F}^{n+1}) = \sum_k \boldsymbol{F}_k^{n+1}\delta_h(\boldsymbol{x}-\boldsymbol{Y}_k^n)\Delta\alpha,$$

$$\mathcal{T}_{1h}(\boldsymbol{u}_{k-1/2}^{n+1}) = \frac{\boldsymbol{U}_k^{n+1}-\boldsymbol{U}_{k-1}^{n+1}}{\Delta s}\cdot\boldsymbol{\tau}_{k-1/2}^n, \qquad \mathcal{T}_{2h}(\boldsymbol{u}_k^{n+1}) = \sum_{\boldsymbol{x}} \boldsymbol{u}^{n+1}(\boldsymbol{x})\delta_h(\boldsymbol{x}-\boldsymbol{Y}_k^n)h^2,$$

$$\langle \boldsymbol{w}, \boldsymbol{v}\rangle_{\Omega_h} = \sum_{\boldsymbol{x}} \boldsymbol{w}(\boldsymbol{x})\cdot\boldsymbol{v}(\boldsymbol{x})h^2, \qquad \langle f, g\rangle_{\Gamma_h} = \sum_k f_{k-1/2}g_{k-1/2}\Delta s, \qquad \langle \phi, \varphi\rangle_{\partial P_h} = \sum_k \phi_{k-1/2}\varphi_{k-1/2}\Delta\alpha.$$

Then we can verify that S_{1h} and $\mathcal{T}_{1h}$ are skew-adjoint, while S_{2h} and $\mathcal{T}_{2h}$ are adjoint as follows:

$$\begin{aligned}
\langle S_{1h}(\sigma^{n+1}), \boldsymbol{u}^{n+1}\rangle_{\Omega_h} &= \sum_{\boldsymbol{x}}\Big(\sum_k D_s(\sigma^{n+1}\boldsymbol{\tau}^n)_k\delta_h(\boldsymbol{x}-\boldsymbol{X}_k^n)\Delta s\Big)\cdot\boldsymbol{u}^{n+1}(\boldsymbol{x})h^2\\
&= \sum_k D_s(\sigma^{n+1}\boldsymbol{\tau}^n)_k\cdot\Big(\sum_{\boldsymbol{x}}\boldsymbol{u}^{n+1}(\boldsymbol{x})\delta_h(\boldsymbol{x}-\boldsymbol{X}_k^n)h^2\Big)\Delta s\\
&= \sum_k D_s(\sigma^{n+1}\boldsymbol{\tau}^n)_k\cdot\boldsymbol{U}_k^{n+1}\Delta s\\
&= \sum_k \frac{\sigma_{k+1/2}^{n+1}\boldsymbol{\tau}_{k+1/2}^n-\sigma_{k-1/2}^{n+1}\boldsymbol{\tau}_{k-1/2}^n}{\Delta s}\cdot\boldsymbol{U}_k^{n+1}\Delta s\\
&= -\sum_k \sigma_{k-1/2}^{n+1}\frac{\boldsymbol{U}_k^{n+1}-\boldsymbol{U}_{k-1}^{n+1}}{\Delta s}\cdot\boldsymbol{\tau}_{k-1/2}^n\Delta s\\
&= \langle\sigma^{n+1}, -\mathcal{T}_{1h}(\boldsymbol{u}^{n+1})\rangle_{\Gamma_h}
\end{aligned}\tag{52}$$

and

$$\begin{aligned}
\langle S_{2h}(\boldsymbol{F}^{n+1}), \boldsymbol{u}^{n+1}\rangle_{\Omega_h} &= \sum_{\boldsymbol{x}}\Big(\sum_k \boldsymbol{F}_k^{n+1}\delta_h(\boldsymbol{x}-\boldsymbol{Y}_k^n)\Delta\alpha\Big)\cdot\boldsymbol{u}^{n+1}(\boldsymbol{x})h^2\\
&= \sum_k \boldsymbol{F}_k^{n+1}\cdot\Big(\sum_{\boldsymbol{x}}\boldsymbol{u}^{n+1}(\boldsymbol{x})\delta_h(\boldsymbol{x}-\boldsymbol{Y}_k^n)h^2\Big)\Delta\alpha\\
&= \langle\boldsymbol{F}^{n+1}, \mathcal{T}_{2h}(\boldsymbol{u}^{n+1})\rangle_{\partial P_h}.
\end{aligned}\tag{53}$$

Indeed, based on these two properties (52) and (53), we are able to rescale the discretizations (24)-(31) to be a symmetric system of linear equations.

4.3. The difference of local stretching factors of two successive time steps is of $O(\Delta t)$

From the moving equation of the elastic interface (42), we have

$$\frac{\boldsymbol{X}_k^{n+1}-\boldsymbol{X}_{k-1}^{n+1}}{\Delta s} = \frac{\boldsymbol{X}_k^n-\boldsymbol{X}_{k-1}^n}{\Delta s} + \Delta t\frac{\boldsymbol{U}_k^{n+1}-\boldsymbol{U}_{k-1}^{n+1}}{\Delta s}\tag{54}$$

and then

$$D_s\boldsymbol{X}_{k-1/2}^{n+1} = D_s\boldsymbol{X}_{k-1/2}^n + \Delta t D_s\boldsymbol{U}_{k-1/2}^{n+1}.\tag{55}$$

By the triangle inequality, we obtain

$$\Big||D_s\boldsymbol{X}_{k-1/2}^{n+1}| - |D_s\boldsymbol{X}_{k-1/2}^n|\Big| \le |D_s\boldsymbol{X}_{k-1/2}^{n+1} - D_s\boldsymbol{X}_{k-1/2}^n| \le \Delta t|D_s\boldsymbol{U}_{k-1/2}^{n+1}|,\tag{56}$$

which shows the difference of local stretching factors of two successive time steps is of $O(\Delta t)$ in the discrete case. Now letting $\Delta s\to 0$, we obtain from (55) that

$$\frac{\partial}{\partial s}\boldsymbol{X}_{k-1/2}^{n+1} = \frac{\partial}{\partial s}\boldsymbol{X}_{k-1/2}^n + \Delta t\frac{\partial}{\partial s}\boldsymbol{U}_{k-1/2}^{n+1},\tag{57}$$

and this leads to

$$\left|\frac{\partial}{\partial s}\boldsymbol{X}_{k-1/2}^{n+1}\right|^2 = \left|\frac{\partial}{\partial s}\boldsymbol{X}_{k-1/2}^n\right|^2 + 2\Delta t\frac{\partial}{\partial s}\boldsymbol{X}_{k-1/2}^n\cdot\frac{\partial}{\partial s}\boldsymbol{U}_{k-1/2}^{n+1} + (\Delta t)^2\left|\frac{\partial}{\partial s}\boldsymbol{U}_{k-1/2}^{n+1}\right|^2.\tag{58}$$

On the other hand, by virtue of (26), we have

$$\begin{aligned}
D_s\boldsymbol{U}_{k-1/2}^{n+1}\cdot D_s\boldsymbol{X}_{k-1/2}^n &= \frac{1}{\sigma_0\Delta t}\Big(\sigma_{k-1/2}^{n+1}-\sigma_{k-1/2}^n\Big)|D_s\boldsymbol{X}_{k-1/2}^n|\\
&= \frac{1}{\Delta t}\Big(\left|\frac{\partial}{\partial s}\boldsymbol{X}_{k-1/2}^{n+1}\right| - \left|\frac{\partial}{\partial s}\boldsymbol{X}_{k-1/2}^n\right|\Big)|D_s\boldsymbol{X}_{k-1/2}^n|,
\end{aligned}\tag{59}$$

which implies

$$\Delta t \frac{\partial}{\partial s}\boldsymbol{X}^n_{k-1/2}\cdot\frac{\partial}{\partial s}\boldsymbol{U}^{n+1}_{k-1/2}=\Big(\Big|\frac{\partial}{\partial s}\boldsymbol{X}^{n+1}_{k-1/2}\Big|-\Big|\frac{\partial}{\partial s}\boldsymbol{X}^{n}_{k-1/2}\Big|\Big)\Big|\frac{\partial}{\partial s}\boldsymbol{X}^{n}_{k-1/2}\Big|. \tag{60}$$

Finally, combining (58) with (60), we have

$$\Big(\Big|\frac{\partial}{\partial s}\boldsymbol{X}^{n+1}_{k-1/2}\Big|-\Big|\frac{\partial}{\partial s}\boldsymbol{X}^{n}_{k-1/2}\Big|\Big)^2=(\Delta t)^2\Big|\frac{\partial}{\partial s}\boldsymbol{U}^{n+1}_{k-1/2}\Big|^2. \tag{61}$$

That is, for the spatial continuous case, the difference of local stretching factors is of $O(\Delta t)$, too.

To conclude this subsection, we summarize that though our formulation (11) allows the interface to be nearly inextensible, from (56), the difference of local stretching factors for two successive time steps is still keeping in $O(\Delta t)$ and the factor $|D^n_s\boldsymbol{X}_{k-1/2}|$ may not be always increasing as much as expected when time step n advances. The spatial continuous case has the similar behavior, see (61). Numerical results reported in Table 5.2 and Figure 5.1 in Section 5 will support this observation. We remark that this result is very different from that of [12].

4.4. The IB discretization scheme (24)-(31) is unconditionally energy stable

In this subsection, we will prove that the IB discretization scheme (24)-(31) is unconditionally stable in the sense that an appropriately defined energy functional associated with the discrete system is decreasing and hence bounded in time [18]. To this goal, we define the spatial-discretized total energy $\mathcal{E}(t)=K_{\mathcal{E}}(t)+P_{\mathcal{E}}(t)$ of the physical system at time t, where the kinetic energy $K_{\mathcal{E}}$ and the potential energy $P_{\mathcal{E}}$ are respectively defined as follows:

$$K_{\mathcal{E}}(t)=\frac{\rho}{2}\langle\boldsymbol{u},\boldsymbol{u}\rangle_{\Omega_h}, \tag{62}$$

$$\begin{aligned}P_{\mathcal{E}}(t)=&\frac{\sigma_0}{2}\Big\langle\Big|\frac{\partial}{\partial s}\boldsymbol{X}(s,t)\Big|-\Big|\frac{\partial}{\partial s}\boldsymbol{X}(s,0)\Big|,\Big|\frac{\partial}{\partial s}\boldsymbol{X}(s,t)\Big|-\Big|\frac{\partial}{\partial s}\boldsymbol{X}(s,0)\Big|\Big\rangle_{\Gamma_h}\\&+\frac{k_0}{2}\langle\boldsymbol{Y}(\alpha,t)-\widetilde{\boldsymbol{Y}}(\alpha,t),\boldsymbol{Y}(\alpha,t)-\widetilde{\boldsymbol{Y}}(\alpha,t)\rangle_{\partial P_h},\end{aligned} \tag{63}$$

where ρ is the fluid density and we have already set, for simplicity, $\rho=1$ in the governing equation (1). We also assume for simplicity that $\boldsymbol{u}=\boldsymbol{0}$ on $\partial\Omega$ for all $t\geq 0$. Now we consider the following kinetic energy estimation:

$$\begin{aligned}K^{n+1}_{\mathcal{E}}-K^n_{\mathcal{E}}&=\frac{1}{2}\langle\boldsymbol{u}^{n+1},\boldsymbol{u}^{n+1}\rangle_{\Omega_h}-\frac{1}{2}\langle\boldsymbol{u}^n,\boldsymbol{u}^n\rangle_{\Omega_h}\\&=\frac{1}{2}\langle\boldsymbol{u}^{n+1}+\boldsymbol{u}^n,\boldsymbol{u}^{n+1}-\boldsymbol{u}^n\rangle_{\Omega_h}\\&=\frac{1}{2}\Big(-\langle\boldsymbol{u}^{n+1}-\boldsymbol{u}^n,\boldsymbol{u}^{n+1}-\boldsymbol{u}^n\rangle_{\Omega_h}+2\langle\boldsymbol{u}^{n+1},\boldsymbol{u}^{n+1}-\boldsymbol{u}^n\rangle_{\Omega_h}\Big)\\&\leq\langle\boldsymbol{u}^{n+1},\boldsymbol{u}^{n+1}-\boldsymbol{u}^n\rangle_{\Omega_h}\\(\text{by (24)})&=\Delta t\langle\boldsymbol{u}^{n+1},\mu\Delta_h\boldsymbol{u}^{n+1}-\nabla_h p^{n+1}+S_{1h}(\sigma^{n+1})+S_{2h}(\boldsymbol{F}^{n+1})\rangle_{\Omega_h}\\(\text{by (25)})&=\Delta t(\boldsymbol{u}^{n+1}_h)^\top(A-\frac{1}{\varepsilon}BB^\top)\boldsymbol{u}^{n+1}_h+\Delta t\langle\boldsymbol{u}^{n+1},S_{1h}(\sigma^{n+1})+S_{2h}(\boldsymbol{F}^{n+1})\rangle_{\Omega_h}.\end{aligned} \tag{64}$$

The potential energy estimation is given by

$$\begin{aligned}P^{n+1}_{\mathcal{E}}-P^n_{\mathcal{E}}&=\frac{1}{2\sigma_0}\langle\sigma^{n+1},\sigma^{n+1}\rangle_{\Gamma_h}-\frac{1}{2\sigma_0}\langle\sigma^n,\sigma^n\rangle_{\Gamma_h}+\frac{1}{2k_0}\langle\boldsymbol{F}^{n+1},\boldsymbol{F}^{n+1}\rangle_{\partial P_h}-\frac{1}{2k_0}\langle\boldsymbol{F}^n,\boldsymbol{F}^n\rangle_{\partial P_h}\\&=\frac{1}{2\sigma_0}\langle\sigma^{n+1}+\sigma^n,\sigma^{n+1}-\sigma^n\rangle_{\Gamma_h}+\frac{1}{2k_0}\langle\boldsymbol{F}^{n+1}+\boldsymbol{F}^n,\boldsymbol{F}^{n+1}-\boldsymbol{F}^n\rangle_{\partial P_h}\\&=\frac{1}{2\sigma_0}\Big(-\langle\sigma^{n+1}-\sigma^n,\sigma^{n+1}-\sigma^n\rangle_{\Gamma_h}+2\langle\sigma^{n+1},\sigma^{n+1}-\sigma^n\rangle_{\Gamma_h}\Big)\end{aligned}$$

$$+\frac{1}{2k_0}\Big(-\langle \boldsymbol{F}^{n+1}-\boldsymbol{F}^n, \boldsymbol{F}^{n+1}-\boldsymbol{F}^n\rangle_{\partial P_h} + 2\langle \boldsymbol{F}^{n+1}, \boldsymbol{F}^{n+1}-\boldsymbol{F}^n\rangle_{\partial P_h}\Big)$$
$$\leq \langle \sigma^{n+1}, \frac{1}{\sigma_0}(\sigma^{n+1}-\sigma^n)\rangle_{\Gamma_h} + \langle \boldsymbol{F}^{n+1}, \frac{1}{k_0}(\boldsymbol{F}^{n+1}-\boldsymbol{F}^n)\rangle_{\partial P_h}.$$

According to (26)-(29), we obtain

$$\begin{aligned} P_{\mathcal{E}}^{n+1} - P_{\mathcal{E}}^n &\leq \langle \sigma^{n+1}, \frac{1}{\sigma_0}(\sigma^{n+1}-\sigma^n)\rangle_{\Gamma_h} + \langle \boldsymbol{F}^{n+1}, \frac{1}{k_0}(\boldsymbol{F}^{n+1}-\boldsymbol{F}^n)\rangle_{\partial P_h} \\ &= \Delta t\langle \sigma^{n+1}, \mathcal{T}_{1h}(\boldsymbol{u}^{n+1})\rangle_{\Gamma_h} - \Delta t\langle \boldsymbol{F}^{n+1}, \mathcal{T}_{2h}(\boldsymbol{u}^{n+1})\rangle_{\partial P_h} \\ &= -\Delta t\langle S_{1h}(\sigma^{n+1}), \boldsymbol{u}^{n+1}\rangle_{\Omega_h} - \Delta t\langle S_{2h}(\boldsymbol{F}^{n+1}), \boldsymbol{u}^{n+1}\rangle_{\Omega_h}. \end{aligned} \tag{65}$$

Now, combining (64) and (65) with the facts that A is negative-definite and $BB^\top$ is positive semi-definite, we have

$$\mathcal{E}^{n+1} - \mathcal{E}^n = (K_{\mathcal{E}}^{n+1} - K_{\mathcal{E}}^n) + (P_{\mathcal{E}}^{n+1} - P_{\mathcal{E}}^n) = \Delta t(\boldsymbol{u}_h^{n+1})^\top (A - \frac{1}{\varepsilon}BB^\top)\boldsymbol{u}_h^{n+1} < 0. \tag{66}$$

In other words, the IB discretization scheme (24)-(31) is unconditionally energy stable.

5 Numerical experiments

In this section, we will perform a series of numerical tests to illustrate the superior performance of the proposed penalty IB method. Throughout this section, except in Example 5, the computational domain is chosen as $\Omega := [-1,1]\times[-1,1]$.

Example 1. (*Convergence test for the Stokes solver*) We first study the convergence behavior of the proposed penalty IB discretization scheme for the steady Stokes problem with $\mu = 1$. The numerical scheme for solving this problem is exactly same as that described in Section 3, except it is steady state and without the elastic interface enclosing a suspended solid particle. We assume that the exact solution $(\boldsymbol{u}, p)$ of the steady Stokes problem is given by (cf. [12])

$$u(x,y) = \sin x\cos y, \quad v(x,y) = -\cos x\sin y, \quad p(x,y) = e^x\sin y.$$

Numerical results for different grid resolutions are reported in Table 5.1. The choice of the penalty parameter $\varepsilon = 10^{-7}$ follows the suggestion given in [6]. From the numerical results, we may observe that the orders of convergence of velocity field is clearly of second-order accuracy, while the pressure is of first-order accuracy. The cause of the first-order convergence of pressure is probably due to that for retaining the symmetry of the resulting linear system (34), we use a first-order extrapolation in the computation of the discrete gradient of pressure $\nabla_h p^{n+1}$ in (24) at the boundary grid points. These results are almost identical with those obtained by the fractional step IB method in [12]. From this observation, we believe that weakening the incompressibility condition from (2) to (17) with a small penalty parameter ε would not be the main source of numerical errors in the immersed boundary approach to fluid-structure interaction problems.

Example 2. (*Convergence test for the Stokes flow with an inextensible interface enclosing a suspended solid particle*) We study the convergence behavior of the Stokes flow with an inextensible interface enclosing a suspended solid particle. For the sake of comparison, we take the kinematic viscosity $\mu = 1$ and in this example, we drop the term $\partial\boldsymbol{u}/\partial t$ from (16) as that of [12]. We put the inextensible interface Γ and the boundary of particle P with initial configurations $\boldsymbol{X}(s,0) = (0.25\cos(s), 0.5\sin(s))$ and $\boldsymbol{Y}(\alpha,0) = (0.1\cos(\alpha), 0.1\sin(\alpha))$ for $0 \leq s, \alpha \leq 2\pi$ under a shear flow $(u,v) = (\gamma y, 0)$ in the fluid domain Ω, where γ is the shear rate. In this example, we take $\gamma = 1$.

Consider the penalty parameters $\varepsilon = 10^{-7}$ and $\sigma_0 = k_0 = 10^7$. We remark that based on our numerical experience, the choices of the penalty parameters are not dependent on the mesh size h and time step Δt.

Table 5.1. Maximum errors of the numerical solution (u_h, v_h, p_h) of Example 1

	$1/h$	$\|u-u_h\|_\infty$	rate	$\|v-v_h\|_\infty$	rate	$\|p-p_h\|_\infty$	rate
	16	1.5782E-04	–	1.5786E-04	–	9.6060E-04	–
Penalty	32	4.4804E-05	1.82	4.4815E-05	1.82	4.2835E-04	1.17
IB method	64	1.2061E-05	1.89	1.2064E-05	1.89	2.0500E-04	1.06
	128	3.1541E-06	1.94	3.1546E-06	1.89	1.0044E-04	1.03
	256	8.1303E-07	1.94	8.1272E-07	1.96	5.1026E-05	0.98
	16	1.5780E-04	–	1.5780E-04	–	9.6150E-04	–
Fractional step	32	4.4810E-05	1.82	4.4810E-05	1.82	4.2860E-04	1.17
IB method [12]	64	1.2060E-05	1.89	1.2060E-05	1.89	2.0520E-04	1.06
	128	3.1530E-06	1.94	3.1530E-06	1.94	1.0050E-04	1.03
	256	8.1200E-07	1.96	8.1200E-07	1.96	4.9700E-05	1.02

Table 5.2. Relative errors of the interface perimeter L_h, maximum errors of the interface configuration $\boldsymbol{X}_h$, and maximum errors of the numerical velocity (u_h, v_h) of Example 2 at time T

	$1/h$	$\|L_0-L_h\|/L_0$	rate	$\|\boldsymbol{X}_{\rm ref}-\boldsymbol{X}_h\|_\infty$	rate	$\|u_{\rm ref}-u_h\|_\infty$	rate	$\|v_{\rm ref}-v_h\|_\infty$	rate
	16	4.7544e-04	–	4.4082e-03	–	6.6113e-02	–	1.3871e-01	–
Penalty	32	2.1585e-04	1.14	1.1455e-03	1.94	2.6011e-02	1.35	4.0193e-02	1.79
IB method	64	1.0411e-04	1.05	4.1673e-04	1.46	1.0095e-02	1.37	1.5367e-02	1.39
($T=0.0625$)	128	5.1292e-05	1.02	1.2945e-04	1.69	3.1458e-03	1.68	4.9530e-03	1.63
	16	3.5110E-02	–	3.4130E-03	–	6.5520E-02	–	1.1330E-01	–
Fractional step	32	2.0890E-02	0.75	1.0790E-03	1.66	2.5920E-02	1.34	3.6600E-02	1.63
IB method [12]	64	1.2200E-02	0.78	4.4380E-04	1.28	1.0530E-02	1.30	1.5540E-02	1.24
($T=0.0625$)	128	6.7490E-03	0.85	1.6220E-04	1.45	4.0470E-03	1.38	4.9680E-03	1.64
	16	4.4363e-03	–	4.2099e-02	–	1.3619e-01	–	1.3717e-01	–
Penalty	32	1.8934e-03	1.23	1.1020e-02	1.93	4.2443e-02	1.68	4.7357e-02	1.53
IB method	64	9.1114e-04	1.06	3.1892e-03	1.79	1.7763e-02	1.26	1.9007e-02	1.32
($T=1$)	128	4.5011e-04	1.02	8.7944e-04	1.86	7.9879e-03	1.15	6.1128e-03	1.64

To examine the convergence rates, we let the mesh size h decrease by half, i.e., $h = 1/16, 1/32, 1/64, 1/128$. We also set the Lagrangian mesh widths to be $\Delta s = \Delta\alpha \approx h/2$ and the time step size $\Delta t = h/4$. Due to the exact solution is not available in this example, we take the result obtained from the finest mesh $h = 1/256$ as our reference solution and compute the errors between the reference and the numerical solutions, although the resulting rate of convergence may tend to be overestimated than the real one. Moreover, since the numerical solutions are not coincide with the same grid locations of the reference solution, we use a linear interpolation to compute the numerical solutions at the desired locations. Let L_0 and A_0 be the perimeter of the interface and the enclosed area at the initial time, while at time t they are denoted by L_h and A_h, respectively.

First, we compute the numerical solutions up to time $T = 0.0625$. At the time, the numerical results produced by the fractional step IB method are available in [12]. The results of both methods are reported in Table 5.2, from which we find that the relative errors of the interface perimeter by the penalty IB method are much smaller than those obtained by the fractional step IB method in [12], and the maximum errors of the interface configuration and the fluid velocity field are comparable with that in [12]. The penalty IB method still can retain reasonable accuracy for a longer time; see the results of time $T = 1$ in Table 5.2. Moreover, from Figure 5.1 for $h = 1/64$ and $T = 20$, we notice that the relative errors of the interface perimeter and enclosed area by the proposed penalty IB method take a rather long time increasing to 10^{-2}. This supports the theoretical finding (56).

Example 3. (*Tank-treading to tumbling motion of a compound interface under shear flow*) In this example, we study the transient deformation from tank-treading to tumbling of an inextensible interface enclosing a suspended solid particle in the simple shear flow with shear rate $\gamma = 1$ and $\mu = 1$. The initial configuration of the interface is given by $\boldsymbol{X}(s, 0) = (0.25\cos(s), 0.5\sin(s))$ for $0 \le s \le 2\pi$. The penalty parameters in the penalty IB method are taken as $\varepsilon = 10^{-7}$ and $\sigma_0 = k_0 = 10^7$. The mesh sizes are chosen as $h = 1/64$, $\Delta s = \Delta\alpha \approx h/2$ and the time step $\Delta t = h/4$.

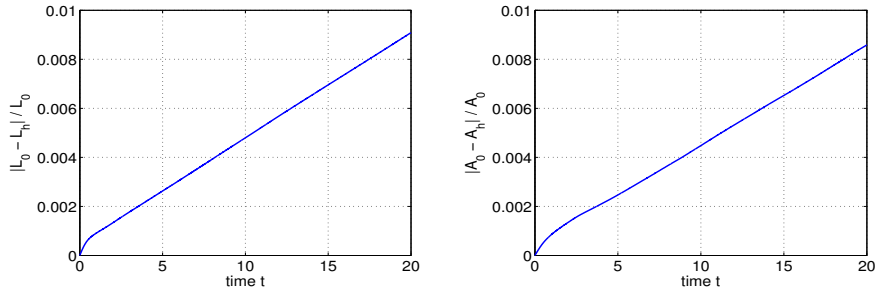

Figure 5.1. Relative errors of the interface perimeter L_h and enclosed area A_h by the penalty IB method with $h = 1/64$ of Example 2 for $0 \le t \le 20$.

We first recall the filling fraction of the solid particle, which is given by $\phi := A_p/A_0$, where A_p and A_0 are respectively the area of solid particle and the enclosed area of interface at the initial time. One of the interesting motions of a compound interface under shear flow is the so-called tank-treading; see Figure 5.2. The tank-treading motion of interface can be characterized by both the inclination angle θ and the tank-treading frequency f of revolution. The former is the angle between the long axis of interface and the flow direction as that shown in Figure 5.2 and the latter is defined as $f = 2\pi/\int_\Gamma (\boldsymbol{u}\cdot\boldsymbol{\tau})^{-1} d\ell$. As it has been pointed out in previous literature [7] [9] [11] [12] [26] [29] that the inclination angle has strongly dependent on the reduced area RA, which is defined as $RA = 4\pi A_0/L_0^2$, but independent on the dimensionless shear rate γ.

We now examine the elastic interface enclosing different solid particles. At first, we consider the case of circular solid particle centered at the origin. Figure 5.3 and Figure 5.5 show the time evolution of the motion for $0 \le t \le 20$ with filling fractions $\phi = 0.08$ and $\phi = 0.42$, respectively. Clearly, the former shows the tank-treading motion, while the latter displays the tumbling. This is consistent with the observation in [27] that the compound interfacial dynamics will have the transition from tank-treading to tumbling if the inclusion effect is strong enough. In other words, if the filling fraction ϕ of the circular solid particle is above some critical threshold, then the interface will start to tumble rather than being stationary. In [12], Lai *et al.* give a possible explanation for this point. By including a solid particle, the energy dissipation enhances, so the compound interface behaves like an inclusion-free interface that encapsulates a more viscous fluid. In some measure, the larger the inclusion is, the higher the viscosity inside the interface will be. The large difference of viscosities of the fluids inside and outside of the interface could eventually cause the transition of motion. Furthermore, we find that a different shape of the enclosed solid particle, even with the same filling fraction, may also result in a different viscosity inside the interface. For example, in Figure 5.6, we consider the interface enclosing a peanut-like solid particle $\boldsymbol{Y}(\alpha, 0) = (0.232\sin(\alpha), 0.38\cos(\alpha)(0.0414 + 0.4004\sin^2(\alpha) - 0.2246\sin^4(\alpha)))$ for $0 \le \alpha \le 2\pi$ with the same filling fraction $\phi = 0.08$ as that investigated in Figure 5.3. However, in this case, the tumbling motion occurs. It is also interesting to point out that although we may observe the tank-treading motion in Figure 5.3, with a close inspection, we find that the inclination angle θ of the compound interface shows a tiny trembling as that depicted in Figure 5.4. This phenomenon can be observed in the inclusion-free case as well.

In this example, we also find that in the tank-treading regime, as the filling fraction increases, both the inclination angle and the tank-treading frequency will decrease. Moreover, the compound interface with larger reduced area has larger inclination angle and tank-treading frequency when the filling fraction is small. These observations are depicted in Figure 5.7. Finally, we investigate the critical value of filling fraction versus the reduced area for the tank-treading to tumbling transition. In Figure 5.8, above the critical value, the interface motion will transit from tank-treading to tumbling. One can easily see that as the reduced area increases, the critical filling fraction increases too. These results are consistent qualitatively with those reported in [12] and [27].

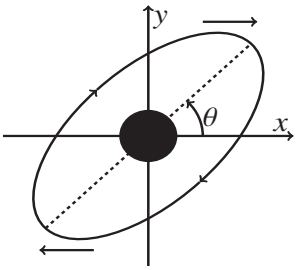

Figure 5.2. (Example 3) Tank-treading motion and inclination angle θ.

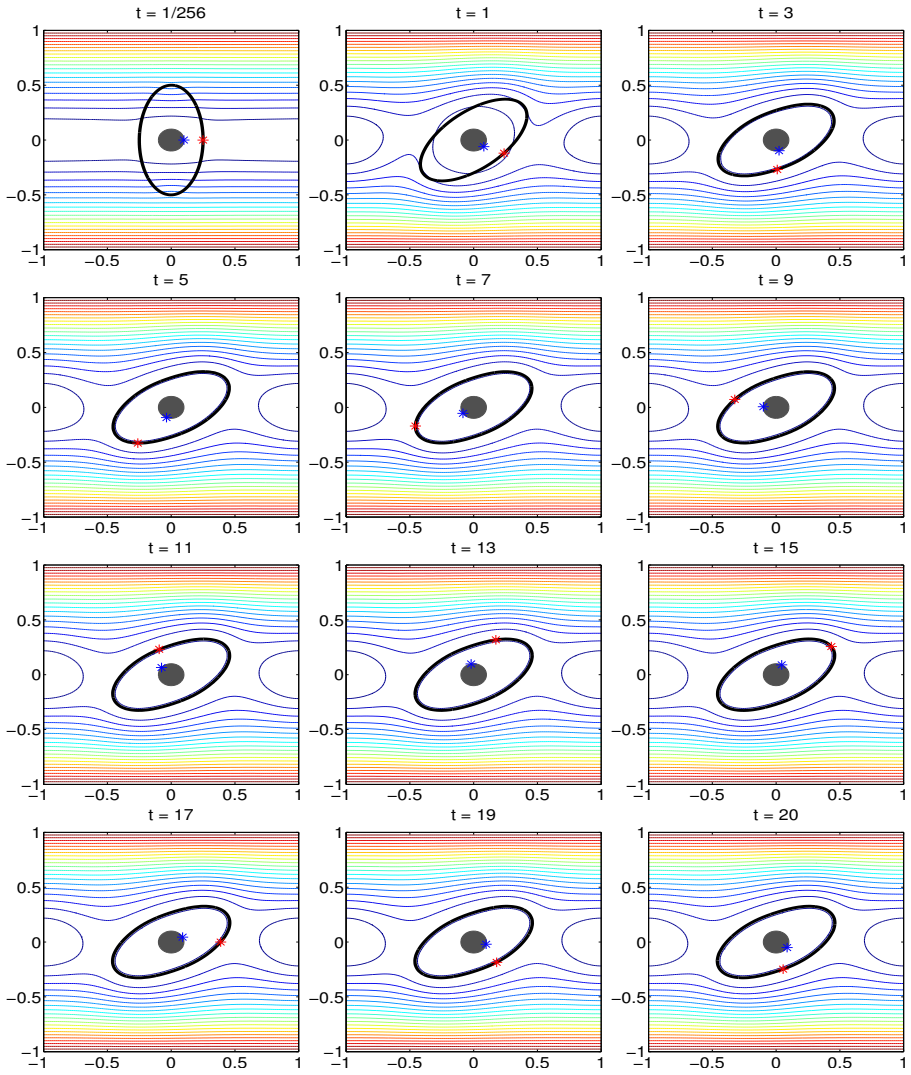

Figure 5.3. (Example 3) The motion of a compound interface in a shear flow with initial configurations $\boldsymbol{X}(s,0) = (0.25\cos(s), 0.5\sin(s))$, $0 \le s \le 2\pi$, and $\boldsymbol{Y}(\alpha,0) = (0.1\cos(\alpha), 0.1\sin(\alpha))$, $0 \le \alpha \le 2\pi$, and filling fraction $\phi = 0.08$.

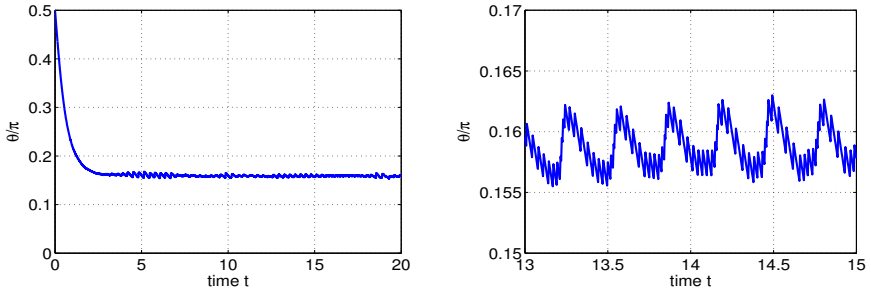

Figure 5.4. (Example 3) The inclination angle θ of a compound interface in a shear flow with initial configurations $\boldsymbol{X}(s,0) = (0.25\cos(s), 0.5\sin(s))$, $0 \le s \le 2\pi$, and $\boldsymbol{Y}(\alpha,0) = (0.1\cos(\alpha), 0.1\sin(\alpha))$, $0 \le \alpha \le 2\pi$, and filling fraction $\phi = 0.08$ for $0 \le t \le 20$ (left) and $13 \le t \le 15$ (right).

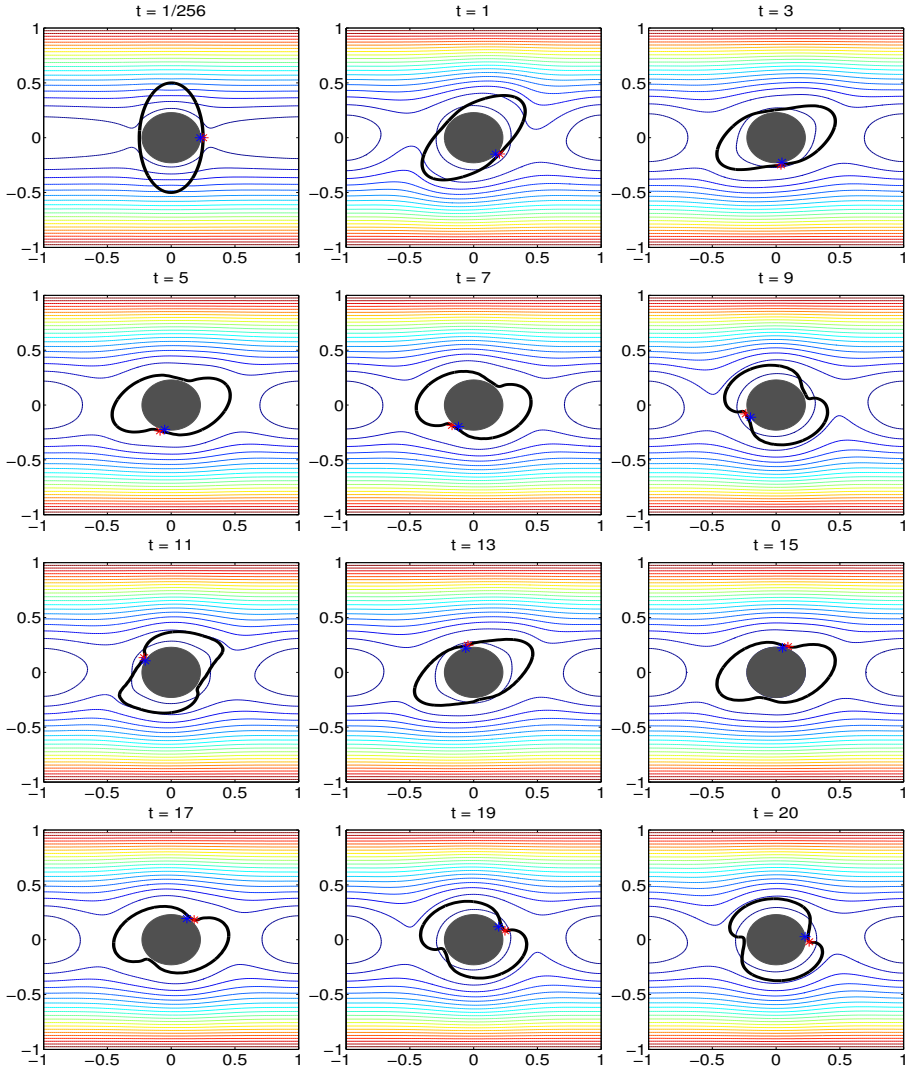

Figure 5.5. (Example 3) The motion of a compound interface in a shear flow with initial configurations $\boldsymbol{X}(s,0) = (0.25\cos(s), 0.5\sin(s))$, $0 \le s \le 2\pi$, and $\boldsymbol{Y}(\alpha,0) = (0.23\cos(\alpha), 0.23\sin(\alpha))$, $0 \le \alpha \le 2\pi$, and filling fraction $\phi = 0.42$.

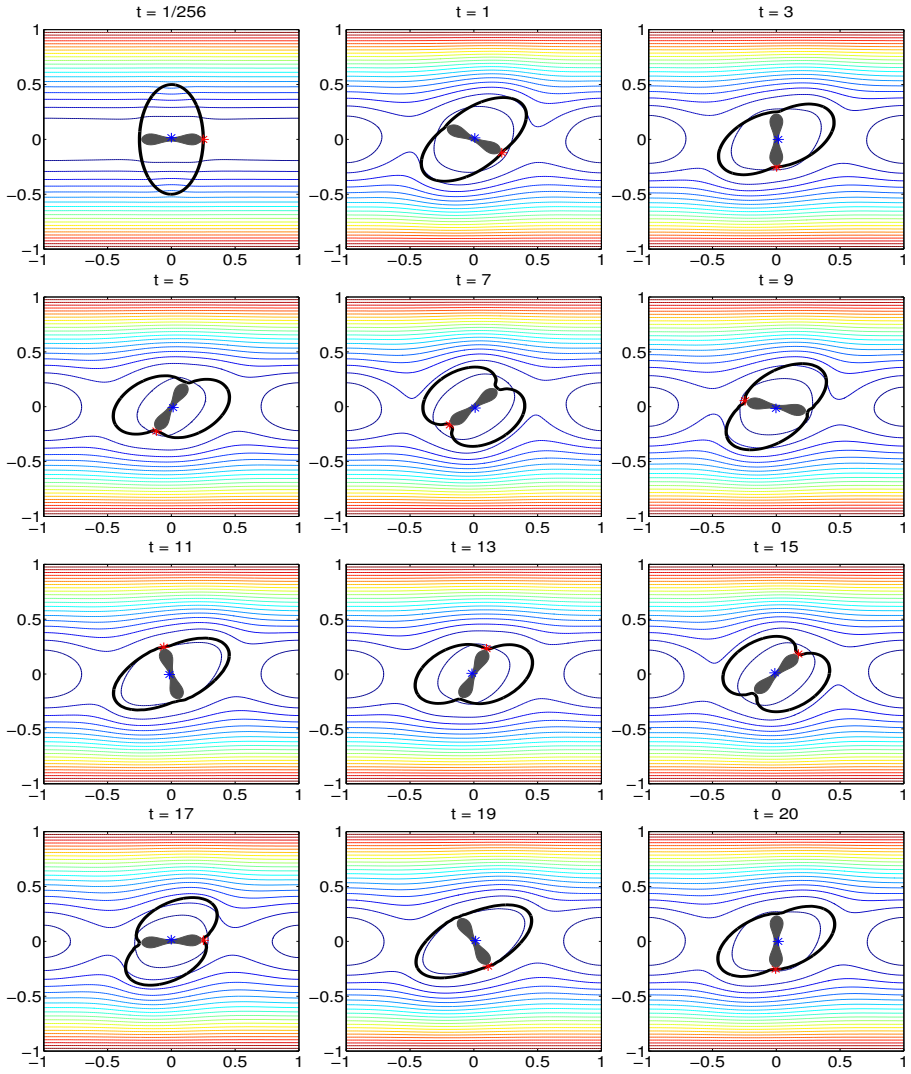

Figure 5.6. (Example 3) The motion of an interface enclosing a peanut-like solid particle in a shear flow with initial configurations $\boldsymbol{X}(s,0) = (0.25\cos(s), 0.5\sin(s))$, $0 \le s \le 2\pi$, and $\boldsymbol{Y}(\alpha,0) = (0.232\sin(\alpha),\ 0.38\cos(\alpha)(0.0414 + 0.4004\sin^2(\alpha) - 0.2246\sin^4(\alpha)))$, $0 \le \alpha \le 2\pi$, and filling fraction $\phi = 0.08$.

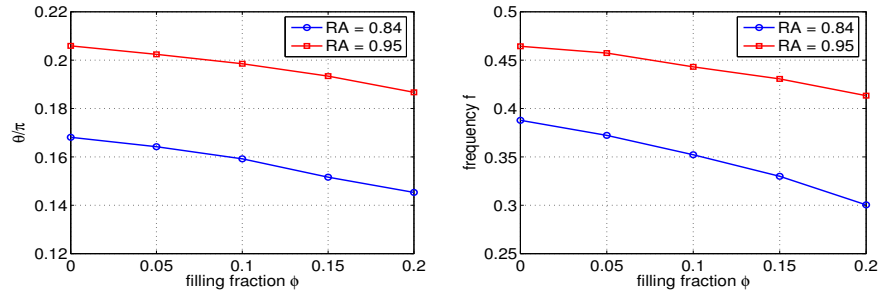

Figure 5.7. (Example 3) The inclination angle θ (left) and tank-treading frequency f (right) versus filling fraction ϕ in the tank-treading regime for two different reduced areas $RA = 0.84$ and $RA = 0.95$.

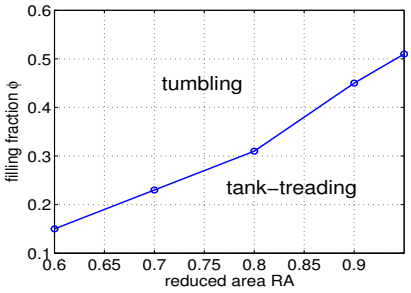

Figure 5.8. (Example 3) The critical filling fraction ϕ for tank-treading to tumbling transition versus reduced area RA.

Example 4. (*Tank-treading to tumbling motion of a compound interface under shear flow by varying the kinematic viscosity* μ) In this example, we investigate the dynamical transition from tank-treading to tumbling of an inextensible interface enclosing a suspended solid particle in the simple shear flow with shear rate $\gamma = 1$ by varying the kinematic viscosity μ. The initial configuration of the interface is given by $\boldsymbol{X}(s,0) = (0.25\cos(s), 0.5\sin(s))$ for $0 \le s \le 2\pi$ enclosing a solid particle whose boundary is parameterized by $\boldsymbol{Y}(\alpha,0) = (0.1\cos(\alpha), 0.1\sin(\alpha))$ for $0 \le \alpha \le 2\pi$. The filling fraction is $\phi = 0.08$. Again, we take the penalty parameters in the penalty IB method as $\varepsilon = 10^{-7}$ and $\sigma_0 = k_0 = 10^7$, and the mesh sizes are chosen as $h = 1/64$, $\Delta s = \Delta\alpha \approx h/2$ and the time step $\Delta t = h/4$.

For the kinematic viscosity $\mu = 1$, the tank-treading motion of the compound interface has been clearly observed in Figure 5.3. The dynamical behavior of $\mu = 0.1$ is very similar to the case of $\mu = 1$. If we decrease μ from 0.01 to 0.001, however, we can find that the transition from tank-treading to tumbling motion occurs; see Figure 5.9 and Figure 5.10. Obviously, the compound interface is easier to tumble when the kinematic viscosity μ is getting smaller.

Example 5. (*Motion of multiple compound vesicles in a shear flow*) In this example, we demonstrate that the proposed penalty IB method can be applied to the problems of multiple vesicles as well. We explore the motion of a group of three identical compound vesicles aligned initially on the x-axis (cf. Figure 5.11) under a shear flow, in which each vesicle is composed of an inextensible interface enclosing a solid particle. The initial configurations of the inextensible interfaces and boundaries of particles are given by

$$\begin{aligned} \boldsymbol{X}_1(s,0) &= (0.2\cos(s) - 0.45, 0.4\sin(s)) \quad \text{and} \quad \boldsymbol{Y}_1(\alpha,0) = (0.08\cos(\alpha) - 0.45, 0.08\sin(\alpha)), \\ \boldsymbol{X}_2(s,0) &= (0.2\cos(s), 0.4\sin(s)) \quad \text{and} \quad \boldsymbol{Y}_2(\alpha,0) = (0.08\cos(\alpha), 0.08\sin(\alpha)), \\ \boldsymbol{X}_3(s,0) &= (0.2\cos(s) + 0.45, 0.4\sin(s)) \quad \text{and} \quad \boldsymbol{Y}_3(\alpha,0) = (0.08\cos(\alpha) + 0.45, 0.08\sin(\alpha)) \end{aligned} \tag{67}$$

for $0 \le s, \alpha \le 2\pi$. Thus, at initial time, one can calculate that the spacing between each pair of interfaces is $1/20$ and and the filling fraction $\phi = 0.08$. We examine the motion of these three compound vesicles under the shear flow $(u, v) = \gamma((1/\pi)\sin\pi y, 0)$ in the fluid domain $[-2, 2] \times [-1, 1]$, where γ is the shear rate. In the simulation, we take $\gamma = 6.25$, the kinematic viscosity $\mu = 1$, the penalty parameters $\varepsilon = 10^{-7}$ and $\sigma_0 = k_0 = 10^7$, and the mesh sizes are chosen as $h = 1/64$, $\Delta s = \Delta\alpha \approx h/2$ and the time step $\Delta t = h/4$. The numerical results are depicted in Figure 5.11, from which we can observe that the group of compound vesicles turns to slant-aligned about time $t = 2.5$ due to the shear flow and then they start to separate. Once they separate, the shear flow will drive the left vesicle toward the lower left corner and the right vesicle to the upper right corner, and the middle one still stands at the origin and displays a tank-treading motion.

We remark that in this example, the computational cost of the proposed penalty method is mainly devoted to solving the the linear system of the velocity approximation at each time step, since the approximations of all other variables can be directly obtained in terms of the approximation of velocity, as that described in Section 3.

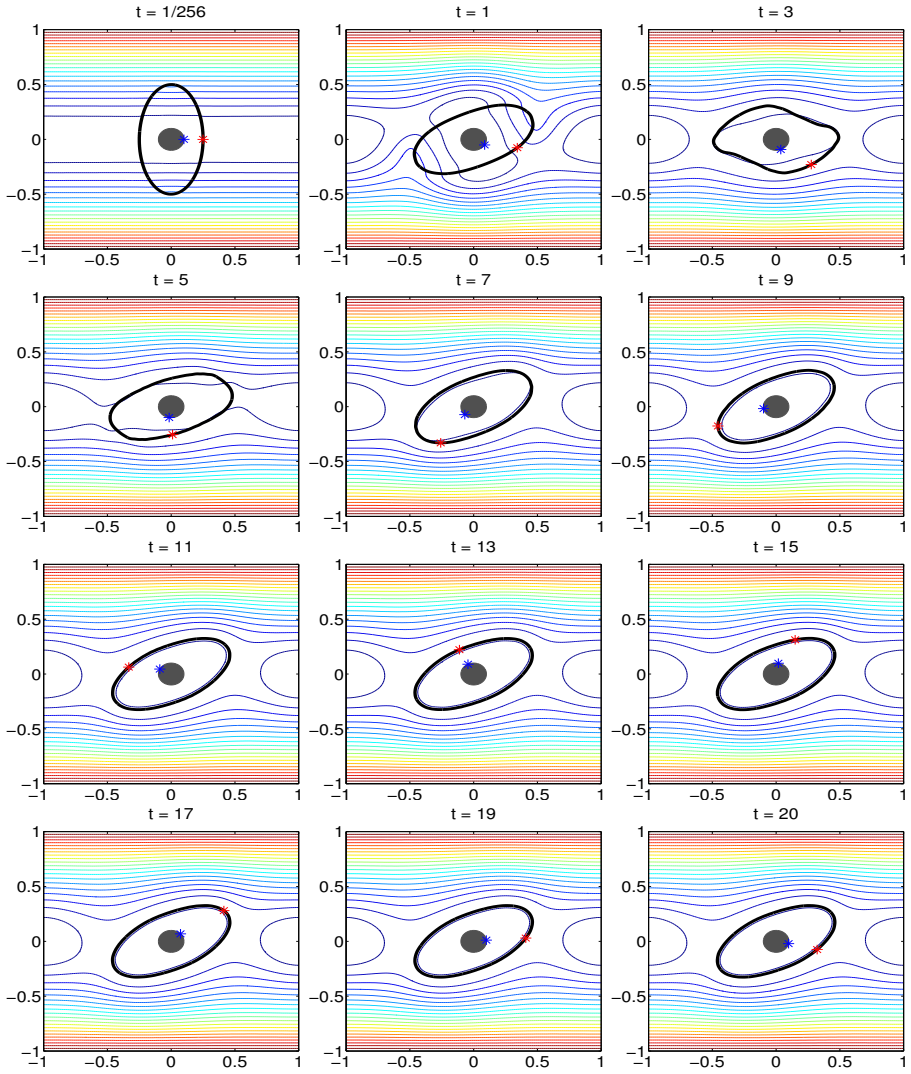

Figure 5.9. (Example 4, $\mu = 0.01$) The motion of a compound interface in a shear flow with initial configurations $\boldsymbol{X}(s,0) = (0.25\cos(s), 0.5\sin(s))$, $0 \le s \le 2\pi$, and $\boldsymbol{Y}(\alpha,0) = (0.1\cos(\alpha), 0.1\sin(\alpha))$, $0 \le \alpha \le 2\pi$, and filling fraction $\phi = 0.08$.

6 Concluding remarks

In this paper, we have proposed a novel penalty IB formulation for simulating the transient Stokes flow with an inextensible interface enclosing a suspended solid particle. The main idea of the proposed approach was based on the penalty techniques by modifying the constitutive equation of Stokes flow to weaken the incompressibility condition, relating the surface divergence to the elastic tension σ to make the interface nearly inextensible, and connecting the particle surface-velocity with the particle surface force $\boldsymbol{F}$ to regularize the particle's rigid motion. The advantage of these regularized governing equations is that when they are discretized by the standard centered difference scheme on a staggered grid, the resulting linear system can easily be reduced by eliminating the unknowns p_h, σ_h and $\boldsymbol{F}_h$ directly. Thus, we just need to solve a smaller linear system of the velocity approximation $\boldsymbol{u}_h$. This advantage can be preserved and even enhanced when such approach is applied to the transient Stokes flow with multiple compound

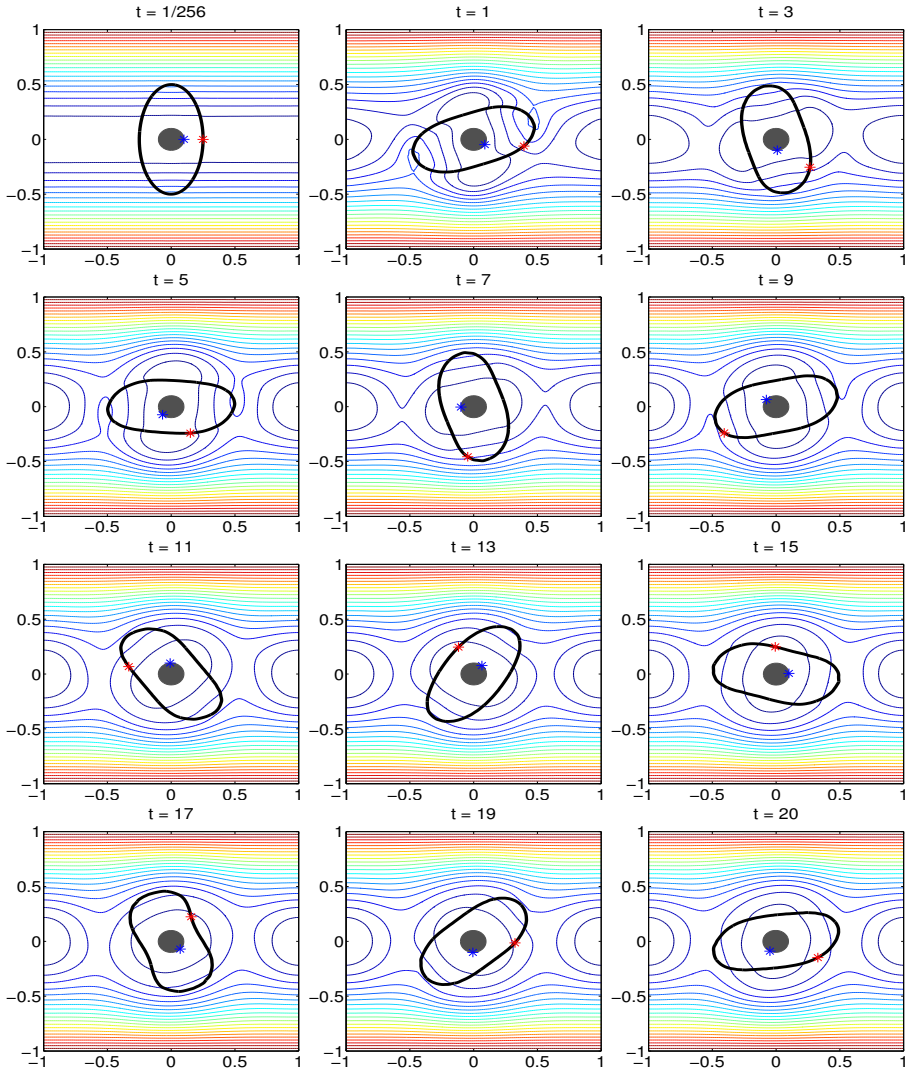

Figure 5.10. (Example 4, $\mu = 0.001$) The motion of a compound interface in a shear flow with initial configurations $\boldsymbol{X}(s,0) = (0.25\cos(s), 0.5\sin(s))$, $0 \le s \le 2\pi$, and $\boldsymbol{Y}(\alpha,0) = (0.1\cos(\alpha), 0.1\sin(\alpha))$, $0 \le \alpha \le 2\pi$, and filling fraction $\phi = 0.08$.

vesicles. Moreover, we have proved that this smaller linear system is symmetric and negative-definite, which enables us to use efficient linear solvers.

One of the advantageous features of the proposed penalty IB method is that the discretization scheme is unconditionally stable in the sense that an appropriately defined energy functional associated with the discrete system is decreasing and hence bounded in time. Another important feature of the approach is that the difference of local stretching factors for two successive time steps is of first order in time step Δt, and the length of the elastic interface may not be always increasing as much as expected when time step advances. We have performed a number of numerical examples to test the accuracy and stability of the IB discretization scheme. The tank-treading and tumbling motions for inextensible interface with a suspended solid particle for different shapes and filling fractions in the simple shear flow have been extensively studied. The simulation of the motion of multiple compound vesicles has been performed as well. Numerical results illustrate the superior performance of the proposed penalty IB method.

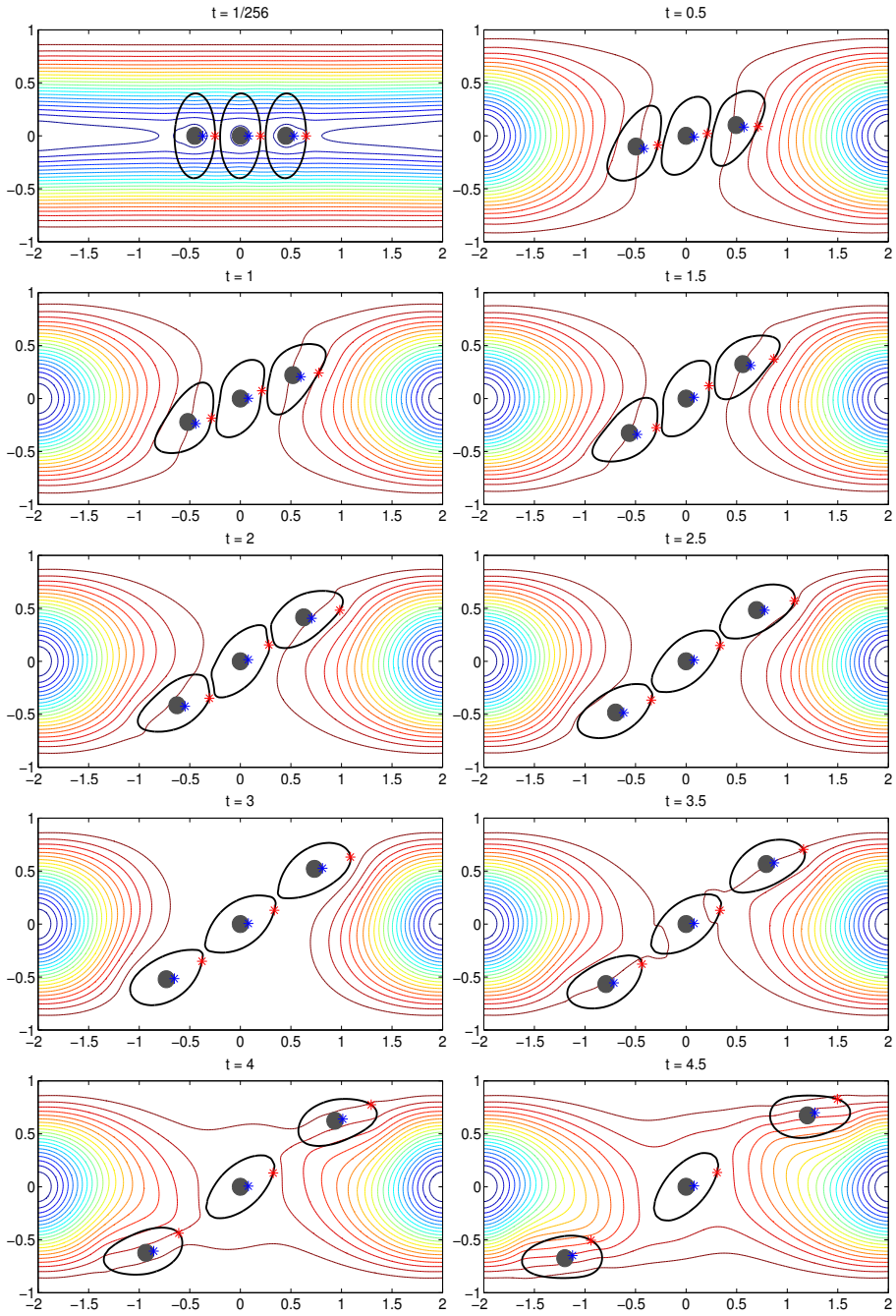

Figure 5.11. (Example 5) The motion of three compound vesicles in a shear flow $(u, v) = 6.25((1/\pi)\sin \pi y, 0)$ with the initial configurations given in (67).

Finally, we remark that the present penalty IB approach can be easily extended to Navier-Stokes flow by treating the nonlinear advection terms explicitly in the time integration.

Acknowledgements The authors would like to thank two anonymous referees for their valuable comments and suggestions that helped to improve the quality of the paper.

References

1. T. Allen and P. Cullis, Drug delivery systems: entering the mainstream, *Science,* 303 (2004), pp. 1818-1822.
2. R. Cortez and M. Minion, The blob projection method for immersed boundary problems, *J. Comput. Phys.,* 161 (2000), pp. 428-453.
3. K. H. de Haas, C. Blom, D. van den Ende, M. H. G. Duits, and J. Mellema, Deformation of giant lipid bilayer vesicles in shear flow, *Phys. Rev. E.,* 56 (1997), pp. 7132-7137.
4. L. J. Fauci and A. L. Fogelson, Truncated newton methods and the modeling of complex immersed elastic structures, *Commun. Pure Appl. Math.,* 66 (1993), pp. 787-818.
5. F. H. Harlow and J. E. Welsh, Numerical calculation of time-dependent viscous incompressible flow of fluid with a free surface, *Phys. Fluids,* 8 (1965), pp. 2181-2189.
6. T. J. R. Hughes, W. K. Liu, and A. Brooks, Finite element analysis of incompressible viscous flows by the penalty function formulation, *J. Comput. Phys.,* 30 (1979), pp. 1-60.
7. V. Kantsler and V. Steinberg, Orientation and dynamics of a vesicle in tank-treading motion in shear flow, *Phys. Rev. Lett.,* 95 (2005), 258101.
8. S. R. Keller and R. Skalak, Motion of a tank-treading ellipsoidal particle in a shear flow, *J. Fluid Mech.,* 120 (1982), pp. 27-47.
9. Y. Kim and M.-C. Lai, Simulating the dynamics of inextensible vesicles by the penalty immersed boundary method, *J. Comput. Phys.,* 229 (2010), pp. 4840-4853.
10. Y. Kim, C. S. Peskin, Penalty immersed boundary method for an elastic boundary with mass, *Phys. Fluids,* 19 (2007), 053103.
11. M. Kraus, W. Wintz, U. Seifert, and R. Lipowsky, Fluid vesicles in shear flow, *Phys. Rev. Lett.,* 77 (1996), pp. 3685-3688.
12. M.-C. Lai, W.-F. Hu, and W.-W. Lin, A fractional step immersed boundary method for stokes flow with an inextensible interface enclosing a solid particle, *SIAM J. Sci. Comput.,* 34 (2012), pp. B692-B710.
13. M.-C. Lai, Y.-H. Tseng, and H. Huang, An immersed boundary method for interfacial flow with insoluble surfactant, *J. Comput. Phys.,* 227 (2008), pp. 7279-7293.
14. R. J. Leveque and Z. Li, Immersed interface methods for Stokes flow with elastic boundaries or surface tension, *SIAM J. Sci. Comput.,* 18 (1997), pp. 709-735.
15. Z. Li and M.-C. Lai, New finite difference methods based on IIM for inextensible interfaces in incompressible flows, *East Asian J. Appl. Math.,* 1 (2011), pp. 155-171.
16. A. A. Mayo and C. S. Peskin, An implicit numerical method for fluid dynamics problems with immersed elastic boundaries, *Contemporary Mathematics,* 141 (1993), pp. 261-277.
17. C. Misbah, Vacillating breathing and tumbling of vesicles under shear flow, *Phys. Rev. Lett.,* 96 (2006), 028104.
18. E. P. Newren, A. L. Fogelson, R. D. Guy, and R. M. Kirby, Unconditionally stable discretizations of the immersed boundary equations, *J. Comput. Phys.,* 222 (2007) pp. 702-719.
19. H. Noguchi and G. Gompper, Swinging and tumbling of fluid vesicles in shear flow, *Phys. Rev. Lett.,* 98 (2007), 128103.
20. C. S. Peskin, The immersed boundary method, *Acta Numerica,* 11 (2002), pp. 479-517.
21. J. S. Sohn, Y.-H. Tseng, S. Li, A. Voigt, and J. S. Lowengrub, Dynamics of multicomponent vesicles in a viscous fluid, *J. Comput. Phys.,* 229 (2010), pp. 119-144.
22. J. M. Stockie and B. R. Wetton, Analysis of stiffness in the immersed boundary method and implications for time-stepping schemes, *J. Comput. Phys.,* 154 (1999), pp. 41-64.
23. K. Taira and T. Colonius, The immersed boundary method: a projection approach, *J. Comput. Phys.,* 225 (2007), pp. 2118-2137.
24. R. Temam, *Navier-Stokes Equations: Theory and Numerical Analysis, Revised Ed.,* Elsevier Science Publishers B.V., Amsterdam, 1984.
25. C. Tu and C. S. Peskin, Stability and instability in the computation of flows with moving immersed boundaries: a comparison of three methods, *SIAM J. Sci. and Stat. Comput.,* 13 (1992), pp. 1361-1376.
26. S. K. Veerapaneni, D. Gueyffier, D. Zorin, and G. Biros, A boundary integral method for simulating the dynamics of inextensible vesicles suspended in a viscous fluid in 2D, *J. Comput. Phys.,* 228 (2009), pp. 2334-2353.
27. S. K. Veerapaneni, Y.-N. Young, P. M. Vlahovska, and J. Blawzdziewicz, Dynamics of a compound vesicle in shear flow, *Phys. Rev. Lett.,* 106 (2011), 158103.
28. X. Yang, X. Zhang, Z. Li, and G.-W. He, A smoothing technique for discrete delta functions with application to immersed boundary method in moving boundary simulations, *J. Comput. Phys.,* 228 (2009), pp. 7821-7836.
29. H. Zhou and C. Pozrikidis, Deformation of liquid capsules with incompressible interfaces in simple shear flow, *J. Fluid Mech.,* 283 (1995), pp. 175-200.